Adaptive modification of lipid droplets mediated by Plin1 functions in infection-induced pathogenesis in *Drosophila*

Lei Wang[1,2,5], Jiaxin Lin[2,3,5], Junjing Yu[4], Zhiqin Fan[2,3], Hong Tang[2 #] and Lei Pan[2,3,6 #]

[1] Wuhan Institute of Virology, Chinese Academy of Sciences, Wuhan, Hubei 430071, China

[2] Key Laboratory of Molecular Virology and Immunology, Institut Pasteur of Shanghai, Chinese Academy of Sciences, Shanghai 200031, China

[3] CAS Center for Excellence in Biotic Interactions, University of Chinese Academy of Sciences, Beijing 100049, China

[4] Shanghai Institute of Biochemistry and Cell Biology, Chinese Academy of Sciences, Shanghai 200031, China.

[5] University of Chinese Academy of Sciences, Beijing 100049, China

[6] Lead contact

#Correspondence: H. Tang (htang@ips.ac.cn) or L. Pan (panlei@ips.ac.cn).

ABSTRACT

Lipid droplets（LDs）are dynamic intracellular organelles critical for lipid metabolism. Alterations in the dynamics and functions of LDs during innate immune response to infections and the underlying mechanisms however, remain largely unknown. Herein, we describe the morphological dynamics of LDs in fat body of *Drosophila*, which vary between transient and sustained bacterial infections. Detailed analysis shows that *perilipin1* (*plin1*), a core gene regulating lipid metabolism of LDs is suppressed by IMD/Relish, an innate immune signaling pathway via Martik (MRT) /Putzig (PZG) complex. During transient immune activation, downregulated *plin1* promotes the formation of large LDs, which alleviates immune reaction-induced reactive oxygen species (ROS) stress. Thus, the growth of LDs is likely an active adaptation to maintain redox homeostasis in response to IMD activation. Whereas, under sustained inflammatory conditions, *plin1* deficiency accelerates excessive decomposition of large LDs through recruitment of Brummer/ATGL lipase resulting in energy wasting, severe lipotoxicity and then deteriorated pathogenesis. Taken together, our study provides evidence that *plin1* has a dual function on LDs' morphology in regulating infection-induced pathogenesis, and Plin1 might be a potential therapeutic target for coordinating inflammation resolution and lipid metabolism.

INTRODUCTION

Immune activation is essentially accompanied by metabolic reprogramming, which redistributes accessible energy to prioritize immune protection against pathogenic infections (Hotamisligil, 2017; O'Neill et al., 2016). Thus, stringent regulation of

46 metabolic machinery in response to immunoreaction is critical for the host fitness.
47 Unlike transient infection, sustained infection is often associated with chronic
48 pathogenesis, which subsequently contributes to metabolic disorders, a major threat to
49 individual health. Besides carbohydrates, lipids provide another important bioenergetic
50 and synthetic resource to the host. A number of lipid metabolites have been reported to
51 play key roles in pro- or anti-inflammatory pathways (Arita, 2012; Serhan et al., 2014;
52 Walpole GFW, 2018). However, the dynamics and differences between lipid
53 metabolism under transient and sustained inflammatory conditions are barely described
54 thus far.
55
56 Lipid droplets（LDs）are important intracellular organelles in all eukaryotic and some
57 prokaryotic cells(Murphy, 2001), providing a major place for lipid synthesis, lysis,
58 transfer and storage. These organelles contain a phospholipid monolayer surrounding
59 neutral lipids, such as di/triacylglycerols or sterol esters (Tauchi-Sato et al., 2002).
60 Since LDs function mainly through storing and providing energy(Walther and Farese,
61 2012), they are apparently involved in multiple physiological and pathological
62 processes in the host. Emerging evidences show that LDs are responsive to ER stress(Fu
63 et al., 2011), buffer starvation stress (Velazquez et al., 2016) and play key roles in
64 diseases such as diabetes and cancer(Cohen JC, 2011; Greenberg et al., 2011). Most
65 intriguingly, LDs also participate in immune regulation including modulation of
66 myeloid cell functions (den Brok et al., 2018), combating pathogenic bacterial
67 infections, being exploited by virus and so on (Saka and Valdivia, 2012; Vallochi et al.,

68 2018; Welte, 2015). The number, size and anchored proteins of LDs are dynamic and
69 change during infection or inflammation (Harsh et al., 2019; Henne et al., 2018; Menon
70 et al., 2019), making it difficult to predict LDs' role as pro- or anti-inflammatory
71 modulators(Pereira-Dutra et al., 2019). It indicates that the status of LDs should be
72 tightly controlled. Defects in the biogenesis and mobilization of LDs result in free fatty
73 acid induced lipotoxicity(Ertunc and Hotamisligil, 2016; Listenberger et al., 2003) or
74 even the accumulation of pro-inflammatory mediators(Feldstein et al., 2004; Summers,
75 2006), all of which lead to metaflammation accompanied by organelles dysfunction,
76 secondary inflammatory responses and exacerbated metabolic dysbiosis (Ertunc and
77 Hotamisligil, 2016). However, the role and dynamic pattern of LDs during immune
78 activation still remains obscure. Especially, the factors mediating this
79 immunometabolic switches of LDs have not been well identified.
80
81 *Drosophila melanogaster* has emerged as a productive organism to investigate
82 immunometabolism, due to the advantages of powerful genetic manipulation and
83 highly conserved mechanisms in both innate immunity and metabolism (Heier and
84 Kuhnlein, 2018; Lemaitre and Hoffmann, 2007; Myllymaki et al., 2014). Especially,
85 the fat body (analogous to human liver and adipose tissue) is an ideal place for studying
86 the interaction between LDs' metabolism and inflammation, due to its richness in LDs
87 and role as a major organ mediating systemic innate immunity(Arrese and Soulages,
88 2010; Kleino and Silverman, 2014). LDs are non-homogenous organelles, which
89 accommodates hundreds of variable proteins (Beller M et al., 2006; Guo Y et al., 2008),

90 including Perilipins (Plins), a group of constitutive proteins that span the surface of LDs
91 (Itabe et al., 2017; Kimmel and Sztalryd, 2016). There are two Plins in *Drosophila*,
92 Lipid storage droplet-1 (*lsd1*, homologous to human PLIN1) and *lsd2* (homologous to
93 human PLIN2) (Bickel et al., 2009). Plin2 acts to promote lipid storage and LDs'
94 growth as a barrier for lipase(Fauny et al., 2005; Grönke et al., 2003; Teixeira et al.,
95 2003), while Plin1 modulates protein flux on LDs(Beller et al., 2010; Bi et al., 2012).
96 In human or mouse adipocyte tissue, PLIN1 deficiency leads to uncontrollable LDs
97 lipolysis and infiltration of inflammatory cells (Gandotra S, 2011; Sohn et al., 2018;
98 Tansey et al., 2001). Inhibition of lipases, such as adipose triglyceride lipase (ATGL)
99 or hormone-sensitive lipase (HSL), can alleviate this metaflammation (Cani et al., 2007;
100 Schweiger et al., 2017). It also indicates a link between immunometabolism and LDs.
101 However, the function of LDs and the underlying mechanisms involving Plins in
102 response to infection are still poorly understood.
103
104 In this study, the dynamic switches in morphology and number of LDs during transient
105 and sustained inflammation, induced either by bacterial infection or genetic
106 manipulation, were compared. Plin1 was found to play a dual role in regulating LDs'
107 morphology under different inflammatory conditions. Our data reveal that adaptive
108 modification of LDs acts as a potential modulator of infection-induced pathogenesis.
109
110 **Results**
111 **Immune activation modulates lipid metabolism, and particularly alters**
112 **morphology of lipid droplets (LDs) in the fat body**.

113 In *Drosophila*, the fat body is not only a central organ mediating systemic immune
114 responses, but also the epicenter for lipid metabolism. Thus, to decipher the mechanistic
115 connections between innate immunity and lipid metabolism, triglycerides (TAGs)
116 kinetics was tested in the fat body of *Drosophila* after systemic infection. Two bacterial
117 species were used to perform nano-injection to infect adult fruit flies. One being the
118 Gram-negative bacterium, *Escherichia. Coli* (*E. coli*), which is non-pathogenic to flies
119 and its infection results in a transient innate immune response within 48 hour post
120 infection (hpi)(Vodovar et al., 2005). Whereas, the Gram-negative bacterium,
121 *Salmonella. Typhimurium* (*S. typhimurium*), which is a deadly pathogen for flies, was
122 used to induce sustained intracellular infection that triggers a prolonged inflammatory
123 response in *Drosophila*(Brandt et al., 2004). The immune deficiency (IMD) pathway is
124 a dominant innate immune singling against Gram-negative bacterial infections that
125 regulates Relish/NF-κB-dependent transcription of AMPs, such as *Diptericin* (*Dpt*)
126 (Hoffmann JA., 2003; JA., 2003; Kaneko T, 2004; Lemaitre and Hoffmann, 2007;
127 Lemaitre, 2007). Thus, by measuring the expression level of *Dpt,* IMD signaling
128 activity could be monitored (Leulier et al., 2003; Neyen et al., 2016). Infection by either
129 bacterial strains led to a gradient increase in IMD activity in the fly fat body from 0 hpi
130 to 12 hpi. However, the transient immune response induced by *E. coli* infection
131 subsided to the basal level after 48 hpi (**Fig.1A**), while activation of IMD continued to
132 increase in case of *Salmonella* infection (**Fig. 1B**). Interestingly, compared to mock
133 injection control (**Supplementary Fig. S1A**), the TAGs level in the fat body of flies
134 with *E.coli* infection steadily increased from 6 hpi to 16 hpi but then declined at 24 hpi

135 and almost recovered after 48 hpi (**Fig. 1A**). In contrast, after *S. typhimurium* infection,
136 TAGs levels continuous decreased in the fat body, which was in negative correlation
137 with the progressive increase in IMD activity (**Fig. 1B**). Moreover, a systemic decrease
138 of TAGs levels was observed in the fly body after *E.coli* infection (**Supplementary Fig.**
139 **S1B**), suggesting a preferred lipid import rather than *de novo* fatty acid synthesis in the
140 fat body from 0 hpi to 12 hpi. This data is consistent with previous studies showing
141 transcriptional levels of most triglyceride synthesis genes are suppressed during the
142 initial phase of infection (Clark et al., 2013; Dionne et al., 2006). While in case of
143 sustained infection by *S. typhimurium,* TAGs levels continuously decreased in the
144 whole body (**Supplementary Fig. 1C**) similar to that observed in the fat body (**Fig.**
145 **1B**). Thus, these results indicate a link between lipid metabolism and IMD signaling
146 activation.
147
148 LDs are the main site for lipid anabolism, catabolism and mobilization(Kühnlein, 2012),
149 which prompted us to investigate whether the morphology of LDs in the fat body
150 responds to bacterial infection. BODIPY staining of fat body cells revealed that
151 compared to PBS injection group (**Fig. 1C and 1C1**), both *E. coli* and *S. typhimurium*
152 infection increased the percentage of intracellular small LDs (diameter < 2 μm) at 6 hpi
153 (**Fig. 1C and 1C2- C3**). In case of *E. coli* infection, however, LDs grew bigger at 16
154 hpi as indicated by the decrease in the percentage small LDs and concurrent increase in
155 large LDs (diameter > 4 μm), and then, this size distribution of LDs was restored to
156 basal levels at 24 hpi (**Fig. 1*C* and 1*C*2**). But after *S. typhimurium* infection, the

157 percentage of small LDs only kept on increasing (**Fig. 1*C* and 1*C*3**). Similar to the
158 changes observed in TAGs levels, the average size of LDs in fat body cells increased
159 till 16 h and then decreased at 24 h post *E. coli* infection, while a continuous decrease
160 was noticed in *S. typhimurium* infection (**Supplementary Fig. S1D**). These results
161 indicate that small LDs are prone to fuse into bigger ones during the initial 16 h of *E.*
162 *coli* infection. On the contrary, large LDs tend to disintegrate during *S. typhimurium*
163 infection (**Fig. 1*C* and Supplementary Fig. S1D**). Together, these results suggest that
164 the morphology of LDs in the fat body changed during bacterial infections and were
165 distinct for transient or sustained immune activation.
166
167 **IMD signaling activation sufficiently modifies the morphology of LD.**
168 To determine whether the IMD activation rather than the potential bacterial effects are
169 responsible for the modification of LDs during infection, a fat body-specific RU486-
170 inducible GAL4 driver (*GS106-GAL4*) (Roman et al., 2001) was applied to detect the
171 relationship between IMD signaling and LDs' patterns in the fat body. Ectopic
172 expression of either different isoforms of *PGRP-LC* (*PGRP-LCx* or *PGRP-LCa*), the
173 receptor for IMD signaling pathway (Choe et al., 2002; He et al., 2017; Yang et al.,
174 2019), or the N-terminal of *Relish* (*Rel.68*), the *Drosophila* NF-kB factor (Wiklund et
175 al., 2009), resulted in constitutive activation of IMD signaling (**Supplementary Fig.**
176 **S1E-G**). IMD activation by *GS106-GAL4* in the fat body led to an increase in TAGs
177 levels in the fat body at 12 h after RU486 treatment (**Fig. 1D and 1E**), simultaneously,
178 the TAGs level of whole body didn't change within 12 hpi (**Supplementary Fig. S1H-**
179 **I**). These results mimicked the phenotypes observed in the early stages (within 12 hours)

180 of transient infection by *E. coli*. However, the elevated levels of TAGs in fat bodies of
181 WT flies disappeared in flies with mutation along IMD signaling pathway (*imd*^{1}、
182 *PGRP-LC*$^{\Delta 5}$ and *relish*^{E20}) at 12h post injection with heat-killed *E. coli* (These immune
183 deficient flies died too quickly when primed by live bacteria.) (**Fig. 1F and**
184 **Supplementary Fig. S1J**). Furthermore, IMD signaling deficiency also restricted the
185 increase in LDs size at 16 hpi, compared to WT controls (**Supplementary Fig. S1K-**
186 **L**). Whereas, prolonged hyper-activation of IMD signaling induced by RU486 (after
187 24 hpi) led to a dramatic decrease in TAGs levels in both fat body and the whole body
188 (**Fig. 1D-E and Supplementary Fig. S1H-I**), accompanied by a decrease in both the
189 percentage of large LDs (**Fig. 1G and 1G1-G3**) and the average LDs size in the fat
190 body (**Fig. 1H**), as observed in sustained infection by *S. typhimurium*. Therefore, these
191 results suggest that IMD activation is necessary and sufficient to modify LDs.
192
193 ***plin1* is involved in LDs modification induced by IMD activation.**
194 To explore the underlying mechanisms of LDs' metabolism in response to immune
195 activation, genes involved in the regulation of LDs (Beller et al., 2010; Grönke et al.,
196 2003; Heier and Kuhnlein, 2018; Kühnlein, 2012) were tested in the fat body by real-
197 time PCR. After comprehensive analysis of mRNA expression, only four genes,
198 *APGAT2, DGAT2, Rfabg* and *plin1* showed opposite transcriptional trends (from 4 hpi
199 to 12 hpi) in transient infection by *E. coli* compared to sustained infection by *S.*
200 *typhimurium* (**Supplementary Fig. S2*A* and S2*B***). Furthermore, we noticed maximum
201 reduction in the expression of *plin1* in the fat body, in which IMD was overactivated
202 through overexpressing *Rel.68* by fat body-specific driver *ppl-GAL4* (**Supplementary**

203 **Fig. S2*C***). These results indicate a potential role of *plin1* in the regulation of LDs'
204 metabolism accompanied by IMD activation.
205
206 Interestingly, similar to the correlation between TAGs level and IMD activity observed
207 in the fat body during bacterial infection of flies (**Fig. 1A**), transient infection of *E. coli*
208 induced a significant downregulation of *plin1* mRNA levels at 4 hpi, which was then
209 restored to basal levels at 24 hpi (**Fig. 2A**). While prolonged activation of IMD
210 signaling either by sustained intracellular *S. typhimurium* infection (**Fig. 2B**), or by
211 RU486 treatment in fat body-specific GS flies (**Fig. 2C**), led to continuous reduction in
212 *plin1* expression. Martik (MRT) /Putzig (PZG) complex, a chromosome remodeling
213 complex, has been reported to suppress *plin1* at transcriptional level (Yao et al., 2018).
214 Intriguingly, mRNA levels of both *mrt* and *pzg* were upregulated in the fat body after
215 bacterial infection (**Fig. 2D and Supplementary Fig. S3A**). Interestingly, homologous
216 alignment showed that at least one conserved binding motif of Relish existed in the
217 promoter region of both *mrt* and *pzg* genes across *Drosophila* species with different
218 evolutionary ages (**Supplementary Fig. S3B and S3C)**. This implies a potential
219 regulation of these genes by IMD/Relish. Peptidoglycan (PGN) derived from gram-
220 negative bacteria can activate IMD signaling in *Drosophila* S2* cells *in vitro* (Kaneko
221 T, 2004). Indeed, luciferase activity controlled by the promoter of *mrt* or *pzg* was
222 significantly enhanced in S2* cells upon PGN treatment, which was blocked by the
223 knockdown of Relish using dsRNA (He et al., 2017) (**Fig. 2E and Supplementary Fig.**
224 **S3D**). Additionally, two Relish binding motifs in truncated *mrt* promoter region (T-

225 *mrt(Rel)*, -870 to +1bp) were critical for *mrt* transcription (**Fig. 2F and Supplementary**
226 **Fig. S3E**), because PGN treatment didn't enhance T-*mrt*-Luc activity any further when
227 these two sites were removed (**Fig. 2F**). Thus, these results suggest that suppression of
228 *plin1* by IMD signaling might be through upregulation of mrt/pzg. Consistent with
229 previous studies (Beller et al., 2010; Bi et al., 2012), *plin1* deficiency by mutation
230 (*plin1*^{38}) or fat body specific knockdown (*UAS-plin1 RNAi* driven by *ppl-GAL4*)
231 promoted the formation of large LDs (**Fig. 2G)**. In contrast, ectopic expression of *plin1*
232 in the fat body enhanced lipid mobilization and inhibited LD coalescence (Yao et al.,
233 2018), leading to the accumulation of small LDs (**Fig. 2G**). All together, these results
234 provide explanation for LDs' growth in the early stages of transient IMD activation.
235
236 **Sustained immune activation accelerates lipolysis of large LDs in a Bmm/ATGL-**
237 **dependent manner.**
238 Unlike transient IMD activation, which promoted LDs' growth (**Fig. 1C and**
239 **Supplementary Fig. S1D**), sustained IMD hyper-activation in the fat body, either
240 driven by *ppl-GAL4* **(Fig. 3A)** or RU486 inducible *GS106-GAL4* for 5 days **(Fig. 3B**
241 **and 3B1)**, accelerated large LDs breakdown and small LDs generation. Simultaneous
242 knockout **(Fig. 3A)** or knockdown **(Fig. 3B)** of *plin1* in the fat body induced the
243 formation of large LDs **(Fig. 3B1)**, albeit the average size of these LDs was smaller
244 than that of flies with *plin1* deficiency alone **(Fig 2G**), but bigger than RU486-untreated
245 controls(**Fig. 3B** and **3B1**). Although these results confirmed the role of Plin1 in
246 reducing LDs' growth, we questioned, why IMD-induced autonomous downregulation

247 of *plin1* was unable to overcome LDs' breakdown in prolonged immune activation
248 conditions. Thus, the long-time course of LDs' morphological change was traced in the
249 fat body of flies with IMD overactivation (*ppl-Gal4>Rel.68*). Although *plin1*
250 deficiency made *ppl-Gal4>Rel.68;plin1*^{38} flies develop much larger LDs than that of
251 *ppl-gal4>Rel.68* at the first week after eclosion, these larger LDs experienced much
252 faster disintegration rate (**Fig. 3C**). Intriguingly, irrespective of the distribution of LDs
253 size (**Fig. 3C1-C2**) or the average LDs size (**Fig. 3D**), there were no significant
254 differences in the fat body of *ppl-GAL4>Rel.68* and *ppl-GAL4>Rel68;plin1*^{38} flies
255 since the second week. Therefore, these results suggest that decomposition of LDs
256 occurs quickly and preferably on large LDs during sustained immune activation.
257
258 Persistent inflammation always over-consumes energy, most of which is produced by
259 lipolysis. Indeed, sustained IMD activation in the fat body (*ppl-GAL4>Rel.68*)
260 enhanced the decrease in TAGs levels in the whole body, which interestingly became
261 much faster in the absence of *plin1* (*ppl-GAL4>Rel68;plin1*^{38}) (**Supplementary Fig.**
262 **S4A**). For further confirmation, these flies were exposed to starvation, a much more
263 sensitive condition. *plin1* mutation dramatically enhanced TAGs consumption rate in
264 *ppl-GAL4>Rel.68;plin1*^{38} flies since the beginning of starvation, compared to *ppl-*
265 *GAL4>Rel.68* flies (**Fig. 3E**). Consequently, flies with a higher TAGs consumption rate
266 were more sensitive to starvation (**Fig. 3F**). A previous study had suggested that LDs
267 lipolysis is predominately mediated by Brummer (Bmm), the *Drosophila* homolog of
268 mammalian adipose TAG lipase (ATGL)(Grönke S, 2007; Gronke et al., 2005). Fat

269 body-specific knockdown of *Bmm* effectively blocked the quick decomposition of large
270 LDs in the fat body of both *ppl-GAL4>Rel.68* and *ppl-GAL4>Rel68;plin1*^{38} flies (**Fig.**
271 **3G**), and further promoted the LDs growth in the fat body (**Fig. 3H)** as well as TAGs
272 content of the whole body **(Supplementary Fig. S4B**). Next, *Bmm-GFP* knock-in
273 allele was used to detect the localization of Bmm on LDs under normal and IMD-
274 activated conditions. Compared to control, IMD activation by fat body-specific
275 overexpression of *Rel.68* significantly enhanced the Bmm-GFP abundance on the
276 surface of LDs. It's worthy to note that Bmm-GFP signals were largely concentrated in
277 the contact site between LDs, a sign of overactive lipolysis (Gronke et al., 2005) (**Fig.**
278 **3I**). Importantly, further removing Plin1 led to a much more recruitment of Bmm-GFP
279 (**Fig. 3I and 3J**). Together, these results suggest that sustained IMD activation enhanced
280 Bmm/ATGL-mediated lipolysis of large LDs.
281
282 ***plin1* compromises host protection against bacterial infection**.
283 Naturally, whether *plin1*-mediated LDs modification participated in the regulation of
284 immune function was tested next. Compared to genetic controls, either *plin1* deficiency
285 (*plin1*^{38}) (**Fig. 4A and 4B**) or fat body-specific knockdown of *plin1* (*ppl-GAL4>UAS-*
286 *plni1RNAi*) (**Fig. 4C and 4D**) prolonged the survival rate and reduced bacterial loads
287 (colony-forming units, CFUs) after *S. typhimurium* systemic infection, indicative of
288 enhanced resistance against bacterial infection. Conversely, ectopic expression of *plin1*
289 in the fat body (*ppl-GAL4>UAS-plin1*) led to a dramatic increase in mortality rate of
290 flies infected with *S. typhimurium* (**Fig. 4E ,** Reducing infection OD because O.E.*plin1*
291 flies died too quickly.**)**, or even by non-pathogenic *E. coli* (**Fig. 4G)**, possibly due to

292 uncontrolled bacterial growth **(Fig. 4F and 4H**). To exclude the potential effects of
293 *plin1* on the development of flies, RU486 induced fat body-specific GAL4 (*GS106-*
294 *GAL4*) was used after fly eclosion. After RU486 treatment for 3 days, a significant
295 decrease or increase in LDs size by overexpression or knockdown of *plin1* respectively,
296 was clearly observed in the fat body (**Fig. 4I**). Subsequently, flies were challenged with
297 *S. typhimurium* and as expected, downregulation of *plin1* prolonged the survival rate,
298 while upregulation of *plin1* shortened the life span and elevated bacterial loads in the *S.*
299 *typhimurium* infected flies (**Fig. 4J and 4K**). However, deficiency of *plin1* did not
300 affect anti-microbial peptides (AMPs) (*Diptericin*, *Dpt; AttacinA, AttA*) response upon
301 *E. coli* infection (**Supplementary Fig. S5A**), but specifically improved *Dpt* expression
302 upon *S. typhimurium* infection (**Supplementary Fig. S5B**). Interestingly,
303 overexpression of *plin1* dampened AMPs response in both *E. coli* and *S. typhimurium*
304 infections (**Supplementary Fig. S5C and S5D**). Taken together, these results suggest
305 that adaptive downregulation of *plin1* in response to IMD signaling activation protected
306 the host against bacterial infections.
307
308 **Large LDs relieves oxidative stress associated with immune activation.**
309 Lipid metabolic disorder usually follows sustained inflammatory response hallmarked
310 by excessive lipolysis-induced lipotoxicity (Blaser et al., 2016; Grisouard et al., 2012;
311 Morgan and Liu, 2011; Zu et al., 2009), which is a causative factor for reactive oxygen
312 species (ROS)-related tissue damage(Ertunc and Hotamisligil, 2016; Herms et al., 2013;
313 Listenberger et al., 2003). Since LDs are major hubs for lipid metabolism in fat body
314 cells, it promoted us to investigate whether *plin1*-mediated LDs modification during

315 immune response regulates intracellular redox homeostasis. A transgenic allele with a
316 *gstD-GFP* insertion was utilized to monitor ROS activity *in vivo* by measuring GFP
317 intensity (Sykiotis and Bohmann, 2008). Transient infection by *E.coli* only induced a
318 slight and temporary elevation of ROS levels in the fat body at 16 hpi. However, *S.*
319 *typhimurium* infection resulted in a continuous and strong increase in intracellular ROS
320 levels in fat bodies (**Fig. 5A and 5A1-A2**). Additionally, fluorescent probe 2',7'-
321 dichlorofluorescein diacetate (DCFH-DA) was also used to evaluate intracellular ROS
322 levels. DCFH-DA staining showed that sustained IMD activation induced by RU486
323 feeding for 5 days caused a significant increase in ROS levels in the fat body of *GS106-*
324 *GAL4>PGRP-LC* (*LCa or LCx*) and *GS106-GAL4>Rel.68* flies (**Fig. 5B and 5B1-B3**).
325 These results suggest a link between sustained IMD activation and accumulation of
326 intracellular oxidative stress. To determine whether immune activation induced-
327 oxidative stress affects the host against bacterial infections, N-acetylcysteine (NAC), a
328 widely-used ROS scavenger, was fed to flies after *S. typhimurium* infection. Feeding
329 flies with NAC specifically at 12 h, not 0h, post *S. typhimurium* infection, a time point
330 when excessive ROS accumulation has already developed (**Fig. 5A**), significantly
331 improved the survival of flies, compared to non-feeding controls (**Fig. 5C**). These
332 results suggest that oxidative stress, which develops during sustained immune response
333 is harmful for the fly after bacterial infection.
334
335 Strikingly, data correlation analysis seemed reveal a positive correlation between the
336 continuously increasing percentages of small LDs (< 2 μm) and the intensity of ROS

337 accumulation in fat body cells after *S. typhimurium* infection (**Fig. 5D**). Considering
338 the phenotypes of low ROS intensity and large LDs formation in WT flies during
339 transient infection by *E. coli* (**Fig. 5A and Fig. 1C**), whether large LDs have the ability
340 to resist intracellular oxidative stress was determined next. *plin1* deficiency (*plin1*^{38}) or
341 knockdown (*UAS-plin1RNAi* driven by *ppl-GAL4*), which promoted LDs growth,
342 contained a lower level of ROS than that of control (**Fig. 5E and 5E1-E2**). In contrast,
343 overexpression of *plin1*（*ppl-GAL4> plin1*）, which transformed LDs into smaller ones,
344 markedly increased ROS intensity (**Fig. 5E and 5E2**). Similar phenotypes were
345 observed in fat body-specific *GS106-GAL4* flies after RU486 induction (**Fig. 5F and**
346 **5F1-F2).** Intriguingly, further removing *plin1* from *ppl-GAL4>Rel.68* flies
347 significantly ameliorated ROS accumulation in the fat body in this sustained IMD
348 activated condition (**Fig. 5G and 5G1**). Importantly, deficiency of *plin1* significantly
349 prolonged the survival of *ppl-GAL4>UAS-Rel.68* flies after *S. typhimurium* infection,
350 with the note that flies with IMD hyper-activation alone (*ppl-GAL4>UAS-Rel.68*) were
351 more susceptible to *S. typhimurium* infection than its genetic controls (**Fig. 5H**). In
352 addition, blocking the breakdown of large LDs associated with IMD overactivation by
353 knockdown of *Bmm* in the fat body, strikingly benefited the survival of *ppl-*
354 *GAL4>Rel.68* flies, even without infection (**Fig. 5I**). Therefore, these results suggest
355 that large LDs formation contribute to alleviate the intracellular oxidative stress induced
356 by IMD activation and Plin1 might serve as an important linker to respond to IMD
357 signaling and modify LDs.
358

359 To further investigate the antioxidative role of LDs, the morphology of LDs in fat body
360 cells was examined in flies with skewed ROS metabolism. In *Drosophila*, superoxide
361 dismutase genes (*sod1/sod2*) or catalase gene (*cat*) encode enzymes for intracellular
362 ROS clearance (C M Griswold et al., 1993; J P Phillips et al., 1989). Knockdown of
363 either *sod1*, *sod2* or *cat* led to excessive ROS accumulation and significantly promoted
364 LDs growth (**Fig. 6A and 6B**). Interestingly, once these flies were fed with NAC to
365 scavenge intracellular ROS, the morphology and the average size of LDs almost
366 reverted to control levels (**Fig. 6A and 6B**). Furthermore, simultaneous overexpression
367 of *plin1* or *Bmm* in the fat body sufficiently blocked the formation of large LDs in *ppl-*
368 *GAL4>UAS-sod1-RNAi*, *sod2-RNAi* or *cat-RNAi* genetic background (**Fig. 6C and 6D**),
369 and as expected led to increased ROS accumulation than controls (**Fig. 6E and 6F**).
370 Taken together, these results suggest that adaptive LDs growth may benefit flies to resist
371 oxidative stress.
372
373
374 **Discussion**
375 Metabolic reprogramming of lipids has been widely reported to be associated with
376 immune responses (Buck et al., 2017; Hotamisligil, 2017; O'Neill et al., 2016). As a
377 major intracellular organelle for lipid metabolism and storage, LDs also seem to be
378 involved in immune processes. Immune stimulation either by infection with bacteria
379 (D'Avila et al., 2006; Peyron et al., 2008), virus (Barba G, 1997; Hope et al., 2002;
380 Samsa et al., 2009), fungus(Sorgi et al., 2009) or protozoan parasites (Vallochi et al.,
381 2018), or by cytokines inoculation (Bandeira-Melo et al., 2001; Pacheco P et al., 2002)

382 may promote the biogenesis of LDs in mammalian leukocytes. Recently, Hash et al also
383 confirmed that LDs are infection-inducible organelles in the gut of *Drosophila* at a
384 certain timepoint after infection (Harsh et al., 2019). However, the status and
385 morphology of LDs change rapidly *in vivo*. This dynamic transformation of LDs during
386 immune response, and their possible link to regulation of pathogenesis is rarely
387 described.
388
389 In this study (**Fig.7**), we carefully traced the time-course morphogenesis of LDs in the
390 fat body beside the dynamic curve of IMD signaling activity. We found that transient
391 IMD activation (within 12hpi) by non-pathogenic bacterial infection promoted LDs'
392 growth in the fat body. The LDs' size and TAGs levels in the fat body was maximum
393 when IMD activity achieved its peak. However, the TAGs level in the whole body
394 decreased around that period, suggesting that the substrates for LDs' biogenesis in the
395 fat body were probably imported lipids rather than *de novo* synthesized fatty acids, and
396 IMD signaling activation is required for this process. Detailed analysis showed that
397 *plin1* downregulation is critical for LDs' growth in response to transient IMD activation,
398 considering its expression was suppressed by IMD/Relish activated MRT/PZG
399 complex. These findings indicate that LDs' biogenesis is likely an active host adaptation
400 to immune challenges. To further support this hypothesis, we found that enlarged LDs
401 benefit the host against intracellular ROS-mediated oxidative stress associated to IMD
402 activation. Excessive ROS accumulation is often the main cause of
403 inflammation/infection-induced cellular damages. A similar antioxidant function of

404 LDs were also reported in neuronal stem cell niche(Bailey et al., 2015) and in cancer
405 cells (Bensaad et al., 2014). However, the detailed mechanisms how large LDs prevent
406 ROS accumulation needs further investigation. One possibility is that biological
407 processes such as cancer, neural activity, and inflammation are energy-intensive, rely
408 on robust fat metabolism, which releases large amounts of free fatty acids. The
409 oxidation of free fatty acids generates ROS and the growth of LDs efficiently sequester
410 these excessive free lipids. Moreover, large LDs' formation can reduce the opportunity
411 of pathogens to utilize free fatty acids for their own growth(Arena et al., 2011; LaRock
412 et al., 2015; Narayanan and Edelmann, 2014). This is possibly the reason why *plin1*
413 deficient flies, owning bigger LDs, had lower bacterial loads after infection. In addition,
414 larger LDs might contain more resident histones, a cationic protein, which has been
415 reported to kill bacteria in a previous study(Anand P et al., 2012). In mammals, IFN-γ
416 treatment of *M. tuberculosis* infected bone-marrow derived macrophage (BMDM) can
417 induce the formation of LDs, in which neutral lipids serve as a source to produce
418 eicosanoids for enhancing host defense (Knight et al., 2018). Thus, LDs' growth is
419 beneficial for both redox homeostasis and to combat infection. The downregulation of
420 Plin1 to promote the enlargement of LDs might be an effective host adaptation to
421 resolve inflammation-associated stress in response to immune activation.
422
423 However, during sustained pathogenesis, induced either by pathogenic bacterial
424 infections or hyper-activation of IMD signaling through genetic manipulation,
425 progressively smaller LDs were observed. We speculate that LDs' growth by

426 autonomous downregulation of endogenous *plin1* in response to IMD activation was
427 unable to overcome LDs' breakdown due to robust lipolysis in high energy-consuming
428 hyperinflammation. Consistent with this idea, the levels of TAGs in the whole body
429 was continuously decreased. Interestingly and impressively, even though the mutation
430 of *plin1* in flies with IMD overactivation enlarged LDs initially, the disintegration of
431 LDs in these flies was rather faster than flies with IMD hyper-activation alone. Protein
432 translocation assay confirmed that *plin1* deficiency increased the recruitment of the key
433 rate-limiting lipase, Bmm/ATGL, on the surface of LDs in sustained IMD
434 overactivation condition. Furthermore, a recent finding showing a higher rate of ATGL-
435 mediated lipolysis in the adipose tissue of *Plin1*$^{-/-}$ mice (Sohn et al., 2018), supports our
436 notion that Bmm/ATGL-mediated lipolysis preferentially occurs in *plin1* deficiency-
437 induced large LDs. As we mentioned above, hyperinflammation leads to excess
438 accumulation of free fatty acids in the cytoplasm, which promote lipotoxicity and ROS-
439 induced oxidative stress(Aitken et al., 2006; Koppers et al., 2010; Song et al., 2014).
440 The high levels of intracellular ROS can further promote lipolysis and free fatty acids
441 release(Krawczyk SA et al., 2012). This vicious circle finally drives the host to enter a
442 severe metaflammatory state during chronic hyperinflammation, and consequently
443 shorten lifespan. A recent study showed that renal purge of hemolymphatic lipids can
444 efficiently prevent ROS-mediated tissue damage during inflammation(Li et al., 2020).
445 In our study, knockdown of Bmm, to prevent free lipids generation, also prolonged the
446 lifespan of flies with hyper-inflammation. Thus, although the growth of LDs was driven
447 by *plin1* downregulation is an active protection mechanism, high energy wasting under

severe pathological conditions is more powerful to consume these large LDs very quickly. Instead, *plin1* mutation seems to enhance the breakdown of large LDs in this case. However, the mechanism of lipase recruitment on large LDs in response to hyper-inflammation, and the involvement of Plin1 require further investigation.

Plin1 is an important protein factor on the surface of LDs. It has been reported to control the mobilization of lipids on LDs surface by recruiting kinds of enzymes(Gandotra et al., 2011; Sztalryd et al., 2003). In this study, we found that *plin1* expression is also regulated by innate immune signaling. This provokes us to conceive that Plin1 may serve as a bridge to link immunity and lipid metabolism through modification of LDs. In response to transient immune activation, adaptative enlarged LDs benefit the host against inflammation-induced stress; while under prolonged hyper-immune activation, large LDs decompose quickly and enhance lipolysis, thus aggravating pathogenesis. The dynamic morphogenesis of LDs under these two conditions are distinctly different, even though both scenarios involve Plin1. It is worthy in the future to trace and dissect the dynamic protein compositions on the surface of LDs along the different stages of inflammation, especially the ones that interact with Plin1. In summary, we found that the homeostasis of LDs' morphology is critical in regulating pathogenesis during infection. Thus, regulation of LDs may provide a potential therapeutic target for resolution of inflammation.

Materials and Methods

470 Detailed information on *Drosophila* stocks and bacterial strain; cloning and double-
471 strand RNAs; infection and survival rate counting; lifespan counting; bacterial loads
472 assay; cell culture, transfection and luciferase assay; qRT-PCR; lipid droplet staining
473 and counting; TAG assay; RU486 treatment; ROS detection; starvation test; microscopy
474 and software; statistical analyses are described in the Supplemental Experimental
475 Procedures.
476

477 **Acknowledgements**

478 We thank Drs. Xun Huang (Institute of Genetics and Developmental Biology, CAS) for
479 providing stocks of *plin1*^{38}, *UAS-plin1* mcherry, *UAS-plin1 RNAi*, *Bmm-GFP* knock-in
480 flies and valuable comments; Yong Liu (Wuhan University) for providing stocks of
481 *UAS-Bmm RNAi* and *UAS-Bmm*. Zhiwei Liu (Shanghai Ocean University) for
482 providing stock of *UAS-gstD-GFP*; Zhihua Liu (Institute of Biophysics, CAS) for
483 providing *S. typhimurium (SR-11)* strain; Ms. Song-qing Liu (Institute of Biophysics,
484 CAS) for fly food preparation and stock maintenance. We thank Dr. Parag Kundu (IPS,
485 CAS) for comments and manuscript polishment. This work was supported by grants
486 from the Strategic Priority Research Program of the Chinese Academy of Sciences to
487 H.T (XDB29030301) and L.P (XDA13010500), Shanghai S&T Innovation Program
488 (2018SHZDZX05) and MOST BR S&T Program (2018ZX10101004002004) to H.T.,
489 the National Natural Science Foundation of China to L.P (31870887) and J.Y
490 (31670909) and Shanghai Municipal Science and Technology Major Project
491 (2019SHZDZX02). L.P is a fellow of CAS Youth Innovation Promotion Association

492 (2012083).

493

494 **Author's contributions**

495 Conceptualization, L.W. and L.P.; Methodology and Validation, L.W. and L.P.; Formal
496 Analysis, L.W. J.L., J.Y., Z.F. and L.P.; Investigation, L.W. and L.P.; Resources, L.P.;
497 Writing-Original Draft, L.W. and L.P.; Writing -Review & Editing, L.P.; Supervision,
498 H.T. and L.P.; Funding Acquisition, J.Y., H.T. and L.P.

499

500 **DECLARATION OF INTERESTS**

501 The authors declare no competing interests.

502

503 **References**

504 Aitken, R.J., Wingate, J.K., De Iuliis, G.N., Koppers, A.J., and McLaughlin, E.A. (2006). Cis-unsaturated
505 fatty acids stimulate reactive oxygen species generation and lipid peroxidation in human spermatozoa.
506 J Clin Endocrinol Metab *91*, 4154-4163.
507 Anand P, Cermelli S, L.Z., Kassan A, Bosch M, S.R., Huang L, Ouellette AJ, Pol A, Welte MA, and SP., G.
508 (2012). A novel role for lipid droplets in the organismal antibacterial response. Elife *13*, e00003.
509 Arena, E.T., Auweter, S.D., Antunes, L.C., Vogl, A.W., Han, J., Guttman, J.A., Croxen, M.A., Menendez, A.,
510 Covey, S.D., Borchers, C.H.*, et al.* (2011). The deubiquitinase activity of the Salmonella pathogenicity
511 island 2 effector, SseL, prevents accumulation of cellular lipid droplets. Infect Immun *79*, 4392-4400.
512 Arita, M. (2012). Mediator lipidomics in acute inflammation and resolution. J Biochem *152*, 313-319.
513 Arrese, E.L., and Soulages, J.L. (2010). Insect fat body: energy, metabolism, and regulation. Annual
514 review of entomology *55*, 207-225.
515 Bailey, A.P., Koster, G., Guillermier, C., Hirst, E.M., MacRae, J.I., Lechene, C.P., Postle, A.D., and Gould,
516 A.P. (2015). Antioxidant Role for Lipid Droplets in a Stem Cell Niche of Drosophila. Cell *163*, 340-353.
517 Bandeira-Melo, C., Phoofolo, M., and Weller, P.F. (2001). Extranuclear lipid bodies, elicited by CCR3-
518 mediated signaling pathways, are the sites of chemokine-enhanced leukotriene C4 production in
519 eosinophils and basophils. The Journal of biological chemistry *276*, 22779-22787.
520 Barba G, H.F., Harada T, Kohara M, Goulinet S, Matsuura Y, Eder G, Schaff Z, Chapman MJ, Miyamura T,
521 Bréchot C. (1997). Hepatitis C virus core protein shows a cytoplasmic localization and associates to
522 cellular lipid storage droplets. Proc Natl Acad Sci U S A *94*, 1200-1205.
523 Beller M, Riedel D, Jänsch L, Dieterich G, Wehland J, Jäckle H, and RP., K. (2006). Characterization of the
524 Drosophila lipid droplet subproteome. Mol Cell Proteomics *6*, 1082-1094.

525 Beller, M., Bulankina, A.V., Hsiao, H.H., Urlaub, H., Jackle, H., and Kuhnlein, R.P. (2010). PERILIPIN-
526 dependent control of lipid droplet structure and fat storage in Drosophila. Cell Metab *12*, 521-532.
527 Bensaad, K., Favaro, E., Lewis, C.A., Peck, B., Lord, S., Collins, J.M., Pinnick, K.E., Wigfield, S., Buffa, F.M.,
528 Li, J.L*., et al.* (2014). Fatty acid uptake and lipid storage induced by HIF-1alpha contribute to cell growth
529 and survival after hypoxia-reoxygenation. Cell reports *9*, 349-365.
530 Bi, J., Xiang, Y., Chen, H., Liu, Z., Gronke, S., Kuhnlein, R.P., and Huang, X. (2012). Opposite and redundant
531 roles of the two Drosophila perilipins in lipid mobilization. J Cell Sci *125*, 3568-3577.
532 Bickel, P.E., Tansey, J.T., and Welte, M.A. (2009). PAT proteins, an ancient family of lipid droplet proteins
533 that regulate cellular lipid stores. Biochimica et biophysica acta *1791*, 419-440.
534 Blaser, H., Dostert, C., Mak, T.W., and Brenner, D. (2016). TNF and ROS Crosstalk in Inflammation. Trends
535 Cell Biol *26*, 249-261.
536 Brandt, S.M., Dionne, M.S., Khush, R.S., Pham, L.N., Vigdal, T.J., and Schneider, D.S. (2004). Secreted
537 Bacterial Effectors and Host-Produced Eiger/TNF Drive Death in aSalmonella-Infected Fruit Fly. PLoS Biol
538 *2*, e418.
539 Buck, M.D., Sowell, R.T., Kaech, S.M., and Pearce, E.L. (2017). Metabolic Instruction of Immunity. Cell
540 *169*, 570-586.
541 C M Griswold, A L Matthews, K E Bewley, and Mahaffey, J.W. (1993). Molecular Characterization and
542 Rescue of Acatalasemic Mutants of Drosophila Melanogaster. Genetics *134(3)*, 781-788.
543 Cani, P.D., Amar, J., Iglesias, M.A., Poggi, M., Knauf, C., Bastelica, D., Neyrinck, A.M., Fava, F., Tuohy, K.M.,
544 Chabo, C*., et al.* (2007). Metabolic endotoxemia initiates obesity and insulin resistance. Diabetes *56*,
545 1761-1772.
546 Choe, K.M., Werner, T., Stoven, S., Hultmark, D., and Anderson, K.V. (2002). Requirement for a
547 peptidoglycan recognition protein (PGRP) in Relish activation and antibacterial immune responses in
548 Drosophila. Science *296*, 359-362.
549 Clark, R.I., Tan, S.W., Pean, C.B., Roostalu, U., Vivancos, V., Bronda, K., Pilatova, M., Fu, J., Walker, D.W.,
550 Berdeaux, R*., et al.* (2013). MEF2 is an in vivo immune-metabolic switch. Cell *155*, 435-447.
551 Cohen JC, H.J., Hobbs HH. (2011). Human Fatty Liver Disease Old Questions and New Insights. Science
552 *6037*, 1519-1523.
553 D'Avila, H., Melo, R.C.N., Parreira, G.G., Werneck-Barroso, E., Castro-Faria-Neto, H.C., and Bozza, P.T.
554 (2006). Mycobacterium bovis Bacillus Calmette-Guerin Induces TLR2-Mediated Formation of Lipid
555 Bodies: Intracellular Domains for Eicosanoid Synthesis In Vivo. The Journal of Immunology *176*, 3087-
556 3097.
557 den Brok, M.H., Raaijmakers, T.K., Collado-Camps, E., and Adema, G.J. (2018). Lipid Droplets as Immune
558 Modulators in Myeloid Cells. Trends Immunol *39*, 380-392.
559 Dionne, M.S., Pham, L.N., Shirasu-Hiza, M., and Schneider, D.S. (2006). Akt and FOXO dysregulation
560 contribute to infection-induced wasting in Drosophila. Curr Biol *16*, 1977-1985.
561 Ertunc, M.E., and Hotamisligil, G.S. (2016). Lipid signaling and lipotoxicity in metaflammation:
562 indications for metabolic disease pathogenesis and treatment. J Lipid Res *57*, 2099-2114.
563 Fauny, J.D., Silber, J., and Zider, A. (2005). Drosophila Lipid Storage Droplet 2 gene (Lsd-2) is expressed
564 and controls lipid storage in wing imaginal discs. Dev Dyn *232*, 725-732.
565 Feldstein, A.E., Werneburg, N.W., Canbay, A., Guicciardi, M.E., Bronk, S.F., Rydzewski, R., Burgart, L.J.,
566 and Gores, G.J. (2004). Free fatty acids promote hepatic lipotoxicity by stimulating TNF-alpha expression
567 via a lysosomal pathway. Hepatology *40*, 185-194.
568 Fu, S., Yang, L., Li, P., Hofmann, O., Dicker, L., Hide, W., Lin, X., Watkins, S.M., Ivanov, A.R., and

569 Hotamisligil, G.S. (2011). Aberrant lipid metabolism disrupts calcium homeostasis causing liver
570 endoplasmic reticulum stress in obesity. Nature *473*, 528-531.
571 Gandotra S, L.D.C., Bottomley W, Cervera P, Giral P, Reznik Y, Charpentier G, Auclair M, Delépine M,
572 Barroso I, Semple RK, Lathrop M, Lascols O, Capeau J, O'Rahilly S, Magré J, Savage DB, Vigouroux C.
573 (2011). Perilipin Deficiency and Autosomal Dominant Partial Lipodystrophy. N Engl J Med *8*, 740.
574 Gandotra, S., Lim, K., Girousse, A., Saudek, V., O'Rahilly, S., and Savage, D.B. (2011). Human frame shift
575 mutations affecting the carboxyl terminus of perilipin increase lipolysis by failing to sequester the
576 adipose triglyceride lipase (ATGL) coactivator AB-hydrolase-containing 5 (ABHD5). The Journal of
577 biological chemistry *286*, 34998-35006.
578 Greenberg, A.S., Coleman, R.A., Kraemer, F.B., McManaman, J.L., Obin, M.S., Puri, V., Yan, Q.W., Miyoshi,
579 H., and Mashek, D.G. (2011). The role of lipid droplets in metabolic disease in rodents and humans. The
580 Journal of clinical investigation *121*, 2102-2110.
581 Grisouard, J., Bouillet, E., Timper, K., Radimerski, T., Dembinski, K., Frey, D.M., Peterli, R., Zulewski, H.,
582 Keller, U., Muller, B*., et al.* (2012). Both inflammatory and classical lipolytic pathways are involved in
583 lipopolysaccharide-induced lipolysis in human adipocytes. Innate Immun *18*, 25-34.
584 Grönke, S., Beller, M., Fellert, S., Ramakrishnan, H., Jäckle, H., and Kühnlein, R.P. (2003). Control of Fat
585 Storage by a Drosophila PAT Domain Protein. Current Biology *13*, 603-606.
586 Grönke S, M.G., Hirsch J, Fellert S, Andreou A, Haase T, Jäckle H, Kühnlein RP. (2007). Dual lipolytic
587 control of body fat storage and mobilization in Drosophila. PLoS Biol *5(6)*, e137.
588 Gronke, S., Mildner, A., Fellert, S., Tennagels, N., Petry, S., Muller, G., Jackle, H., and Kuhnlein, R.P. (2005).
589 Brummer lipase is an evolutionary conserved fat storage regulator in Drosophila. Cell metabolism *1*,
590 323-330.
591 Guo Y, Walther TC, Rao M, Stuurman N, Goshima G, Terayama K, Wong JS, Vale RD, Walter P, and RV., F.
592 (2008). Functional genomic screen reveals genes involved in lipid-droplet formation and utilization.
593 Nature *7195*, 657-661.
594 Harsh, S., Heryanto, C., and Eleftherianos, I. (2019). Intestinal lipid droplets as novel mediators of host-
595 pathogen interaction in Drosophila. Biol Open *8*.
596 He, X., Yu, J., Wang, M., Cheng, Y., Han, Y., Yang, S., Shi, G., Sun, L., Fang, Y., Gong, S.T*., et al.* (2017).
597 Bap180/Baf180 is required to maintain homeostasis of intestinal innate immune response in Drosophila
598 and mice. Nat Microbiol *2*, 17056.
599 Heier, C., and Kuhnlein, R.P. (2018). Triacylglycerol Metabolism in Drosophila melanogaster. Genetics
600 *210*, 1163-1184.
601 Henne, W.M., Reese, M.L., and Goodman, J.M. (2018). The assembly of lipid droplets and their roles in
602 challenged cells. EMBO J *37*.
603 Herms, A., Bosch, M., Ariotti, N., Reddy, B.J., Fajardo, A., Fernandez-Vidal, A., Alvarez-Guaita, A.,
604 Fernandez-Rojo, M.A., Rentero, C., Tebar, F*., et al.* (2013). Cell-to-cell heterogeneity in lipid droplets
605 suggests a mechanism to reduce lipotoxicity. Curr Biol *23*, 1489-1496.
606 Hoffmann JA. (2003). The immune response of Drosophila. Nature *426*, 33-38.
607 Hope, R.G., Murphy, D.J., and McLauchlan, J. (2002). The domains required to direct core proteins of
608 hepatitis C virus and GB virus-B to lipid droplets share common features with plant oleosin proteins.
609 The Journal of biological chemistry *277*, 4261-4270.
610 Hotamisligil, G. (2017). Foundations of Immunometabolism and Implications for Metabolic Health and
611 Disease. Immunity *3*, 406-420.
612 Itabe, H., Yamaguchi, T., Nimura, S., and Sasabe, N. (2017). Perilipins: a diversity of intracellular lipid

613 droplet proteins. Lipids in health and disease *16*, 83.
614 J P Phillips , S D Campbell, D Michaud, M Charbonneau, and Hilliker, A.J. (1989). Null Mutation of Copper-
615 Zinc Superoxide Dismutase in Drosophila Confers Hypersensitivity to Paraquat and Reduced Longevity.
616 Proc Natl Acad Sci *86(8)*, 2761-2765.
617 JA., H. (2003). The immune response of Drosophila. Nature *426*, 33-38.
618 Kaneko T, G.W., Mellroth P, Steiner H, Fukase K, Kusumoto S, Harley W, Fox A, Golenbock D, Silverman
619 N. (2004). Monomeric and polymeric gram-negative peptidoglycan but not purified LPS stimulate the
620 Drosophila IMD pathway. Immunity *20*, 637-649.
621 Kimmel, A.R., and Sztalryd, C. (2016). The Perilipins: Major Cytosolic Lipid Droplet-Associated Proteins
622 and Their Roles in Cellular Lipid Storage, Mobilization, and Systemic Homeostasis. Annual review of
623 nutrition *36*, 471-509.
624 Kleino, A., and Silverman, N. (2014). The Drosophila IMD pathway in the activation of the humoral
625 immune response. Developmental and comparative immunology *42*, 25-35.
626 Knight, M., Braverman, J., Asfaha, K., Gronert, K., and Stanley, S. (2018). Lipid droplet formation in
627 Mycobacterium tuberculosis infected macrophages requires IFN-gamma/HIF-1alpha signaling and
628 supports host defense. PLoS Pathog *14*, e1006874.
629 Koppers, A.J., Garg, M.L., and Aitken, R.J. (2010). Stimulation of mitochondrial reactive oxygen species
630 production by unesterified, unsaturated fatty acids in defective human spermatozoa. Free Radic Biol
631 Med *48*, 112-119.
632 Krawczyk SA, Haller JF, Ferrante T, Zoeller RA, and BE, C. (2012). Reactive Oxygen Species Facilitate
633 Translocation of Hormone Sensitive Lipase to the Lipid Droplet During Lipolysis in Human Differentiated
634 Adipocytes. PLoS ONE *7*, e34904.
635 Kühnlein (2012). Thematic review series: Lipid droplet synthesis and metabolism: from yeast to man.
636 Lipid droplet-based storage fat metabolism in Drosophila. J Lipid Res *53(8)*, 1430-1436.
637 LaRock, D.L., Chaudhary, A., and Miller, S.I. (2015). Salmonellae interactions with host processes. Nat
638 Rev Microbiol *13*, 191-205.
639 Lemaitre, B., and Hoffmann, J. (2007). The host defense of Drosophila melanogaster. Annual review of
640 immunology *25*, 697-743.
641 Lemaitre, B.a.H., J., (2007). The host defense of Drosophila melanogaster. Annual review of immunology
642 *25*, 697-743.
643 Leulier, F., Parquet, C., Pili-Floury, S., Ryu, J.H., Caroff, M., Lee, W.J., Mengin-Lecreulx, D., and Lemaitre,
644 B. (2003). The Drosophila immune system detects bacteria through specific peptidoglycan recognition.
645 Nature immunology *4*, 478-484.
646 Li, X., Rommelaere, S., Kondo, S., and Lemaitre, B. (2020). Renal Purge of Hemolymphatic Lipids Prevents
647 the Accumulation of ROS-Induced Inflammatory Oxidized Lipids and Protects Drosophila from Tissue
648 Damage. Immunity *52*, 374-387 e376.
649 Listenberger, L.L., Han, X., Lewis, S.E., Cases, S., Farese, R.V., Jr., Ory, D.S., and Schaffer, J.E. (2003).
650 Triglyceride accumulation protects against fatty acid-induced lipotoxicity. Proc Natl Acad Sci U S A *100*,
651 3077-3082.
652 Menon, D., Singh, K., Pinto, S.M., Nandy, A., Jaisinghani, N., Kutum, R., Dash, D., Prasad, T.S.K., and
653 Gandotra, S. (2019). Quantitative Lipid Droplet Proteomics Reveals Mycobacterium tuberculosis
654 Induced Alterations in Macrophage Response to Infection. ACS infectious diseases *5*, 559-569.
655 Morgan, M.J., and Liu, Z.G. (2011). Crosstalk of reactive oxygen species and NF-kappaB signaling. Cell
656 Res *21*, 103-115.

657 Murphy, D. (2001). The biogenesis and functions of lipid bodies in animals, plants and microorganisms.
658 Prog Lipid Res *5*, 325-438.
659 Myllymaki, H., Valanne, S., and Ramet, M. (2014). The Drosophila imd signaling pathway. J Immunol *192*,
660 3455-3462.
661 Narayanan, L.A., and Edelmann, M.J. (2014). Ubiquitination as an efficient molecular strategy employed
662 in salmonella infection. Front Immunol *5*, 558.
663 Neyen, C., Runchel, C., Schüpfer, F., Meier, P., and Lemaitre, B. (2016). The regulatory isoform rPGRP-LC
664 induces immune resolution via endosomal degradation of receptors. Nature immunology *17*, 1150-1158.
665 O'Neill, L.A., Kishton, R.J., and Rathmell, J. (2016). A guide to immunometabolism for immunologists.
666 Nature reviews Immunology *16*, 553-565.
667 Pacheco P, Bozza FA, G.R., Bozza M, W.P., Castro-Faria-Neto HC, and PT., B. (2002). Lipopolysaccharide-
668 induced leukocyte lipid body formation in vivo innate immunity elicited intracellular Loci involved in
669 eicosanoid metabolism.pdf>. J Immunol *1*, 6498-6506.
670 Pereira-Dutra, F.S., Teixeira, L., de Souza Costa, M.F., and Bozza, P.T. (2019). Fat, fight, and beyond: The
671 multiple roles of lipid droplets in infections and inflammation. Journal of leukocyte biology.
672 Peyron, P., Vaubourgeix, J., Poquet, Y., Levillain, F., Botanch, C., Bardou, F., Daffe, M., Emile, J.F., Marchou,
673 B., Cardona, P.J.*, et al.* (2008). Foamy macrophages from tuberculous patients' granulomas constitute a
674 nutrient-rich reservoir for M. tuberculosis persistence. PLoS Pathog *4*, e1000204.
675 Roman, G., Endo, K., Zong, L., and Davis, R.L. (2001). P[Switch], a system for spatial and temporal control
676 of gene expression in Drosophila melanogaster. Proceedings of the National Academy of Sciences of the
677 United States of America *98*, 12602-12607.
678 Saka, H.A., and Valdivia, R. (2012). Emerging roles for lipid droplets in immunity and host-pathogen
679 interactions. Annu Rev Cell Dev Biol *28*, 411-437.
680 Samsa, M.M., Mondotte, J.A., Iglesias, N.G., Assuncao-Miranda, I., Barbosa-Lima, G., Da Poian, A.T.,
681 Bozza, P.T., and Gamarnik, A.V. (2009). Dengue virus capsid protein usurps lipid droplets for viral particle
682 formation. PLoS pathogens *5*, e1000632.
683 Schweiger, M., Romauch, M., Schreiber, R., Grabner, G.F., Hutter, S., Kotzbeck, P., Benedikt, P., Eichmann,
684 T.O., Yamada, S., Knittelfelder, O.*, et al.* (2017). Pharmacological inhibition of adipose triglyceride lipase
685 corrects high-fat diet-induced insulin resistance and hepatosteatosis in mice. Nature communications *8*,
686 14859.
687 Serhan, C.N., Chiang, N., Dalli, J., and Levy, B.D. (2014). Lipid mediators in the resolution of inflammation.
688 Cold Spring Harb Perspect Biol *7*, a016311.
689 Sohn, J.H., Lee, Y.K., Han, J.S., Jeon, Y.G., Kim, J.I., Choe, S.S., Kim, S.J., Yoo, H.J., and Kim, J.B. (2018).
690 Perilipin 1 (Plin1) deficiency promotes inflammatory responses in lean adipose tissue through lipid
691 dysregulation. J Biol Chem.
692 Song, Y., Li, X., Li, Y., Li, N., Shi, X., Ding, H., Zhang, Y., Li, X., Liu, G., and Wang, Z. (2014). Non-esterified
693 fatty acids activate the ROS-p38-p53/Nrf2 signaling pathway to induce bovine hepatocyte apoptosis in
694 vitro. Apoptosis *19*, 984-997.
695 Sorgi, C.A., Secatto, A., Fontanari, C., Turato, W.M., Belanger, C., de Medeiros, A.I., Kashima, S., Marleau,
696 S., Covas, D.T., Bozza, P.T.*, et al.* (2009). Histoplasma capsulatum cell wall {beta}-glucan induces lipid body
697 formation through CD18, TLR2, and dectin-1 receptors: correlation with leukotriene B4 generation and
698 role in HIV-1 infection. J Immunol *182*, 4025-4035.
699 Summers, S.A. (2006). Ceramides in insulin resistance and lipotoxicity. Prog Lipid Res *45*, 42-72.
700 Sykiotis, G.P., and Bohmann, D. (2008). Keap1/Nrf2 signaling regulates oxidative stress tolerance and

701 lifespan in Drosophila. Dev Cell *14*, 76-85.
702 Sztalryd, C., Xu, G., Dorward, H., Tansey, J.T., Contreras, J.A., Kimmel, A.R., and Londos, C. (2003).
703 Perilipin A is essential for the translocation of hormone-sensitive lipase during lipolytic activation. The
704 Journal of cell biology *161*, 1093-1103.
705 Tansey, J.T., Sztalryd, C., Gruia-Gray, J., Roush, D.L., Zee, J.V., Gavrilova, O., Reitman, M.L., Deng, C.X., Li,
706 C., Kimmel, A.R.*, et al.* (2001). Perilipin ablation results in a lean mouse with aberrant adipocyte lipolysis,
707 enhanced leptin production, and resistance to diet-induced obesity. Proc Natl Acad Sci U S A *98*, 6494-
708 6499.
709 Tauchi-Sato, K., Ozeki, S., Houjou, T., Taguchi, R., and Fujimoto, T. (2002). The surface of lipid droplets is
710 a phospholipid monolayer with a unique Fatty Acid composition. The Journal of biological chemistry
711 *277*, 44507-44512.
712 Teixeira, L.s., Rabouille, C., Rørth, P., Ephrussi, A., and Vanzo, N.F. (2003). Drosophila Perilipin/ADRP
713 homologue Lsd2 regulates lipid metabolism. Mechanisms of Development *120*, 1071-1081.
714 Vallochi, A.L., Teixeira, L., Oliveira, K.D.S., Maya-Monteiro, C.M., and Bozza, P.T. (2018). Lipid Droplet, a
715 Key Player in Host-Parasite Interactions. Front Immunol *9*, 1022.
716 Velazquez, A.P., Tatsuta, T., Ghillebert, R., Drescher, I., and Graef, M. (2016). Lipid droplet-mediated ER
717 homeostasis regulates autophagy and cell survival during starvation. The Journal of cell biology *212*,
718 621-631.
719 Vodovar, N., Vinals, M., Liehl, P., Basset, A., Degrouard, J., Spellman, P., Boccard, F., and Lemaitre, B.
720 (2005). Drosophila host defense after oral infection by an entomopathogenic Pseudomonas species.
721 Proceedings of the National Academy of Sciences of the United States of America *102*, 11414-11419.
722 Walpole GFW, G.S., Westman J. (2018). The Role of Lipids in Host–PathogenInteractions. IUBMB Life *5*,
723 384-392.
724 Walther, T.C., and Farese, R.V., Jr. (2012). Lipid droplets and cellular lipid metabolism. Annual review of
725 biochemistry *81*, 687-714.
726 Welte, M.A. (2015). Expanding roles for lipid droplets. Current biology : CB *25*, R470-481.
727 Wiklund, M.L., Steinert, S., Junell, A., Hultmark, D., and Stoven, S. (2009). The N-terminal half of the
728 Drosophila Rel/NF-kappaB factor Relish, REL-68, constitutively activates transcription of specific Relish
729 target genes. Developmental and comparative immunology *33*, 690-696.
730 Yang, S., Zhao, Y., Yu, J., Fan, Z., Gong, S.T., Tang, H., and Pan, L. (2019). Sugar Alcohols of Polyol Pathway
731 Serve as Alarmins to Mediate Local-Systemic Innate Immune Communication in Drosophila. Cell Host
732 Microbe *26*, 240-251 e248.
733 Yao, Y., Li, X., Wang, W., Liu, Z., Chen, J., Ding, M., and Huang, X. (2018). MRT, Functioning with NURF
734 Complex, Regulates Lipid Droplet Size. Cell Rep *24*, 2972-2984.
735 Zu, L., He, J., Jiang, H., Xu, C., Pu, S., and Xu, G. (2009). Bacterial endotoxin stimulates adipose lipolysis
736 via toll-like receptor 4 and extracellular signal-regulated kinase pathway. J Biol Chem *284*, 5915-5926.

737

738 **MAIN FIGURES AND LEGENDS**

739 Including seven main figures.

740

Figure 1

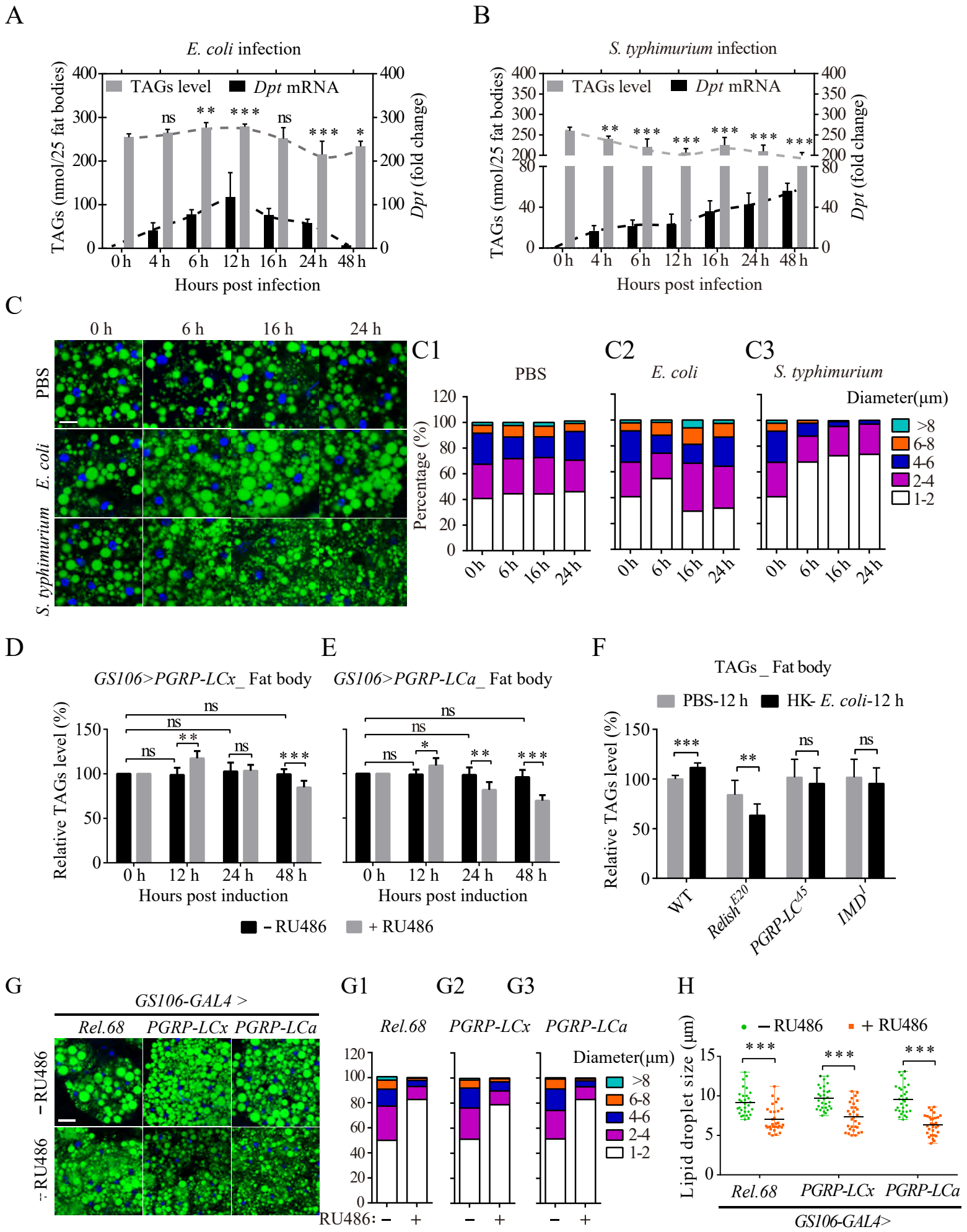
A
E. coli infection
TAGs level
Dpt mRNA
TAGs (nmol/25 fat bodies)
Dpt (fold change)
Hours post infection
B
S. typhimurium infection
C
0 h
6 h
16 h
24 h
PBS
E. coli
S. typhimurium
C1
C2
C3
Percentage (%)
Diameter(μm)
>8
6-8
4-6
2-4
1-2
D
GS106>PGRP-LCx_ Fat body
Relative TAGs level (%)
Hours post induction
E
GS106>PGRP-LCa_ Fat body
F
TAGs _ Fat body
PBS-12 h
HK- E. coli-12 h
WT
Relish E20
PGRP-LC Δ5
IMD 1
– RU486
+ RU486
G
GS106-GAL4 >
Rel.68
PGRP-LCx
PGRP-LCa
G1
G2
G3
RU486:
H
Lipid droplet size (μm)
GS106-GAL4>

Fig. 1. IMD signaling activation switches lipid metabolism and LDs morphology in the fat body. (**A** and **B**) Relative *Dptericin*(*Dpt*) mRNA expression and TAGs level in the fat body of wild type flies at indicated time points post *E. coli* (**A**) and *S. typhimurium* (**B**) infection. The mean values of *Dpt* mRNA expression or TAGs level were connected by dash line. The fold change of mRNA expression was normalized to that of 0 h and four independent repeats (n =20 flies per repeat) were performed at each time point. Total TAGs level of 25 flies' fat body tissues was quantified in six biological replicates at each time point. (**C**) BODIPY staining (green) of LDs in the fat body of wild type flies at indicated time points post *E. coli* (upper panel) and *S. typhimurium* (lower panel) infection. Nuclei of fat body cells were stained with DAPI (blue). Scale bar: 10 μm. The corresponding statistics of the distribution of LDs' size was shown in (**C1**) for *E. coli* infection and in (**C2**) for *S. typhimurium* infection (n =30 cells for each time point). Eight fat bodies were examined for each time point. (**D** and **E**) Relative changes of TAGs level in the fat body of *GS106-GAL4> PGRP-LCx* (**D**) and *GS106-GAL4> PGRP-LCa* (**E**) flies after RU486 treatment for indicated time. The change of TAG levels was normalized to that of 0h without RU486 treatment. Six independent repeats (n =25 flies per repeat) at each time point were performed. (**F**) Relative TAGs level in the fat body of wild type and IMD pathway mutants (*Relish*， *PGRP-LC* and *Imd*). Each value of TAGs level was normalized to that of 0h of wild type. Each data contains four independent repeats (25 flies' fat body tissues per repeat). (**G**) BODIPY staining (green) of LDs in the fat body of indicated flies after 5 days with (lower panel) or without (upper panel) RU486 treatment (**G**). Nuclei of fat body cells were stained with DAPI (blue). Scale bar: 20 μm. The corresponding statistics of the distribution of LDs' size was shown in (**G1**) for *GS106-GAL4> Rel.68* flies, in (**G2**) for *GS106-GAL4> PGRP-LCx* flies and in (**G3**) for *GS106-GAL4> PGRP-LCa* flies (n =30 cells in each genotype). Eight fat bodies were examined for each sample. (**H**) The statistics of LDs size (n =30 cells) in fat body cells of indicated flies after RU486 treatment for 5 days. Each scattering dot represents the data from one fat body cell. Error bars represent the mean ± s.d. (**A-B, D-F**) and mean with range (**H**). Data were analyzed by One-way ANOVA with Tukey's multiple-comparison test (**A-B, D, E**) and Multiple t-tests (**D-F, H**). $*p < 0.05$; $**p < 0.01$; $***p < 0.001$; ns, not significant. **See also in Supplementary Figure 1.**

Figure 2

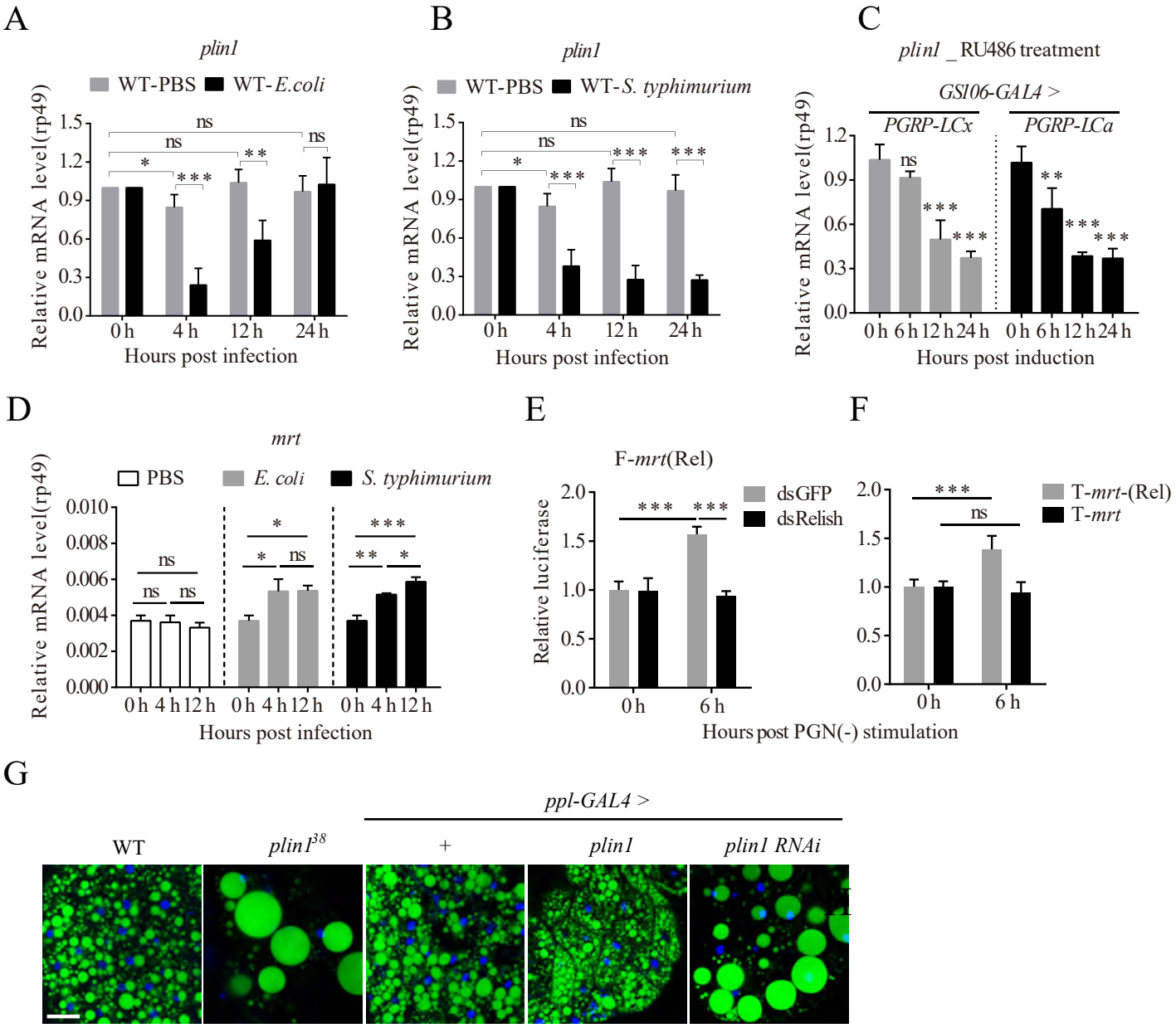
A
plin1
WT-PBS
WT-E.coli
Relative mRNA level(rp49)
Hours post infection
B
plin1
WT-PBS
WT-S. typhimurium
Relative mRNA level(rp49)
Hours post infection
C
plin1 _RU486 treatment
GSl06-GAL4 >
PGRP-LCx
PGRP-LCa
Relative mRNA level(rp49)
Hours post induction
D
mrt
PBS
E. coli
S. typhimurium
Relative mRNA level(rp49)
Hours post infection
E
F-mrt(Rel)
dsGFP
dsRelish
Relative luciferase
F
T-mrt-(Rel)
T-mrt
Hours post PGN(-) stimulation

G

ppl-GAL4 >
WT
plin1^38
+
plin1
plin1 RNAi

Fig. 2. *plin1* responds to IMD activation through Mrt/Pzg complex, and regulates LDs' morphology. (**A and B**) Relative *plin1* mRNA levels in the fat body of wild type flies at the indicated time points post *E. coli* (**A**) or *S. typhimurium* (**B**) infection. Flies treated with sterile PBS were used as a control. The fold change of mRNA expression was normalized to that of 0 h**.** (**C**) Relative *plin1* mRNA levels in the fat body of *GS106-GAL4>PGRP-LCs* flies after RU486 treatment for indicated time. The fold change of mRNA expression was normalized to that of 0 h. (**D**) Relative *mrt* mRNA levels in the fat body of wild type flies post *E. coli* or *S. typhimurium* infection. Flies treated with sterile PBS were used as a control. The fold change of mRNA expression was normalized to that of 0 h. (**E**) Relative luciferase activities of F-*mrt*(Rel) (Full length promoter of -1.5kb to +1bp including all predicted Relish Binding motifs in Fig. S3) reporter in S2* cells after double strand RNA (dsRNA) and PGN (35 μg/ml) treatment. All data were normalized to dsGFP control group at 0 h. Three independent repeats were performed at each time point for each treatment. (**F**) Relative luciferase activities of T-*mrt*(Rel) (Truncated length promoter of -870 to +1bp with two key binding motifs) and T-*mrt* (Truncated length promoter with no binding motifs) reporter in S2* cells after PGN (35 μg/ml) treatment. All data were normalized to T-*mrt*(Rel) group at 0 h. Three independent repeats were performed at each time point for each group. (**G**) BODIPY staining (green) of LDs in the fat body of indicated flies. Nuclei of fat body cells were stained with DAPI (blue). Eight fat bodies were examined for each genotype. Scale bar: 20 μm. Error bars represent the mean ± s.d.. Data were analyzed by One-way ANOVA with Tukey's multiple-comparison test (**A-D**), Multiple t-tests (**A-B**) and Student's t test (**E-F**). $*p < 0.05$; $**p < 0.01$; $***p < 0.001$; ns, no significance. **See also in Supplementary Figure 2 and 3.**

Figure 3

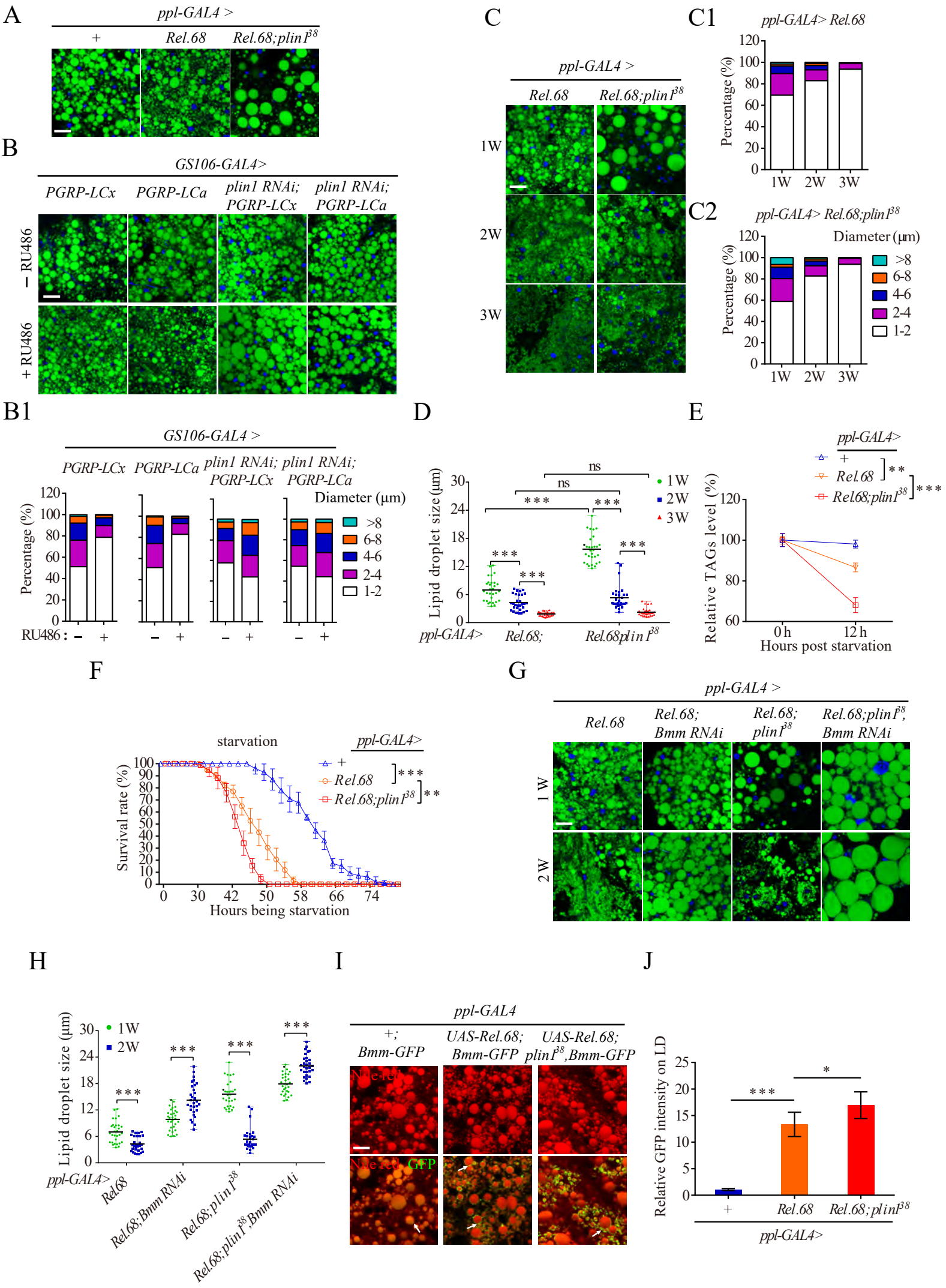
A
ppl-GAL4 >
+
Rel.68
Rel.68;plin1^38
B
GS106-GAL4>
PGRP-LCx
PGRP-LCa
plin1 RNAi; PGRP-LCx
plin1 RNAi; PGRP-LCa
– RU486
+ RU486
B1
GS106-GAL4 >
Percentage (%)
Diameter (μm)
>8
6-8
4-6
2-4
1-2
RU486 : – +
C
ppl-GAL4 >
Rel.68
Rel.68;plin1^38
1W
2W
3W
C1
ppl-GAL4> Rel.68
Percentage (%)
1W 2W 3W
C2
ppl-GAL4> Rel.68;plin1^38
Diameter (μm)
D
Lipid droplet size (μm)
1W
2W
3W
ns
***
ppl-GAL4>
Rel.68;
Rel.68plin1^38
E
ppl-GAL4>
+
Rel.68
Rel.68;plin1^38
**
***
Relative TAGs level (%)
0 h
12 h
Hours post starvation
F
starvation
ppl-GAL4>
+
Rel.68
Rel.68;plin1^38
***
**
Survival rate (%)
Hours being starvation
G
ppl-GAL4 >
Rel.68
Rel.68; Bmm RNAi
Rel.68; plin1^38
Rel.68;plin1^38, Bmm RNAi
1 W
2 W
H
Lipid droplet size (μm)
1W
2W
***
ppl-GAL4>
Rel.68
Rel.68;Bmm RNAi
Rel.68;plin1^38
Rel.68;plin1^38;Bmm RNAi
I
ppl-GAL4
+; Bmm-GFP
UAS-Rel.68; Bmm-GFP
UAS-Rel.68; plin1^38,Bmm-GFP
Nile red
Nile red, GFP
J
Relative GFP intensity on LD
***
*
+
Rel.68
Rel.68;plin1^38
ppl-GAL4>

Fig. 3. *S*ustained IMD activation prefers to enhance Bmm-mediated lipolysis on large LDs. (**A**) BODIPY staining (green) of LDs in the fat body of indicated flies. Nuclei of fat body cells were stained with DAPI (blue). Eight fat bodies were examined for each genotype. Scale bar: 20 μm. (**B**) BODIPY staining (green) of LDs (**B**) and statistics of the size distribution of LDs (**B1**) in the fat body of indicated flies after RU486 treatment for 5 days. Nuclei of fat body cells were stained with DAPI (blue). Eight fat bodies were examined for each sample. Scale bar: 20 μm. (**C** and **D**) BODIPY staining (green) of LDs in the fat body of *ppl-GAL4>Rel.68* and *ppl-GAL4>Rel.68,plin*^{38} adult flies (up panel, one-week age; middle panel, two-week age; low panel, three-week age). The corresponding statistics of the distribution of LDs' size was shown in (**C1**) for *ppl-GAL4>Rel.68* flies and in (**C2**) for *ppl-GAL4>Rel.68,plin*^{38} flies (n =30 cells), and the corresponding statistics of the average size of LDs (**D**). Nuclei of fat body cells were stained with DAPI (blue). Eight fat bodies were examined for each sample. Scale bars: 20 μm. (**E**) Relative TAGs level in the whole body of indicated flies before/after starvation. The change of TAG levels was normalized to that of 0 h for each genotype. Six independent replicates for each sample were performed (n =12 per repeat). (**F**) Survival curves of indicated flies (n = 60) with starvation. (**G** and **H**) BODIPY staining (green) of LDs (**G**) and the corresponding statistics of the average size of LDs (n =30 cells) (**H**) in the fat body of indicated adult flies (up panel, one-week age; low panel, two-week age). Eight fat bodies were examined for each sample. Each scattering dot represents the data from one fat body cell. Nuclei of fat body cells were stained with DAPI (blue). Scale bars: 20 μm. (**I-J**) Nile red staining (red) of LDs and imaging of GFP signals (green) around LDs in the fat body of Bmm-GFP knock-in flies (**I**), and quantification of GFP intensity on the surface of lipid droplet (**J**). The GFP enrichment indicated by arrow is a sign of lipolysis. Eight fat bodies were examined for each genotype. Scale bars: 10 μm. Values of plotted curves represent mean ± s.d. of at least three independent repeats (**E-F**). Error bars represent the mean with range (**D, H**) and mean ± s.d. (**J**). Data were analyzed by Student t-tests (**D-E, J**), Multiple t-tests (**H**) and Kaplan – Meier (**F**). $^{**}p < 0.01$; $^{***}p < 0.001$; ns, no significance. **See also in Supplementary Figure 4.**

Figure 4

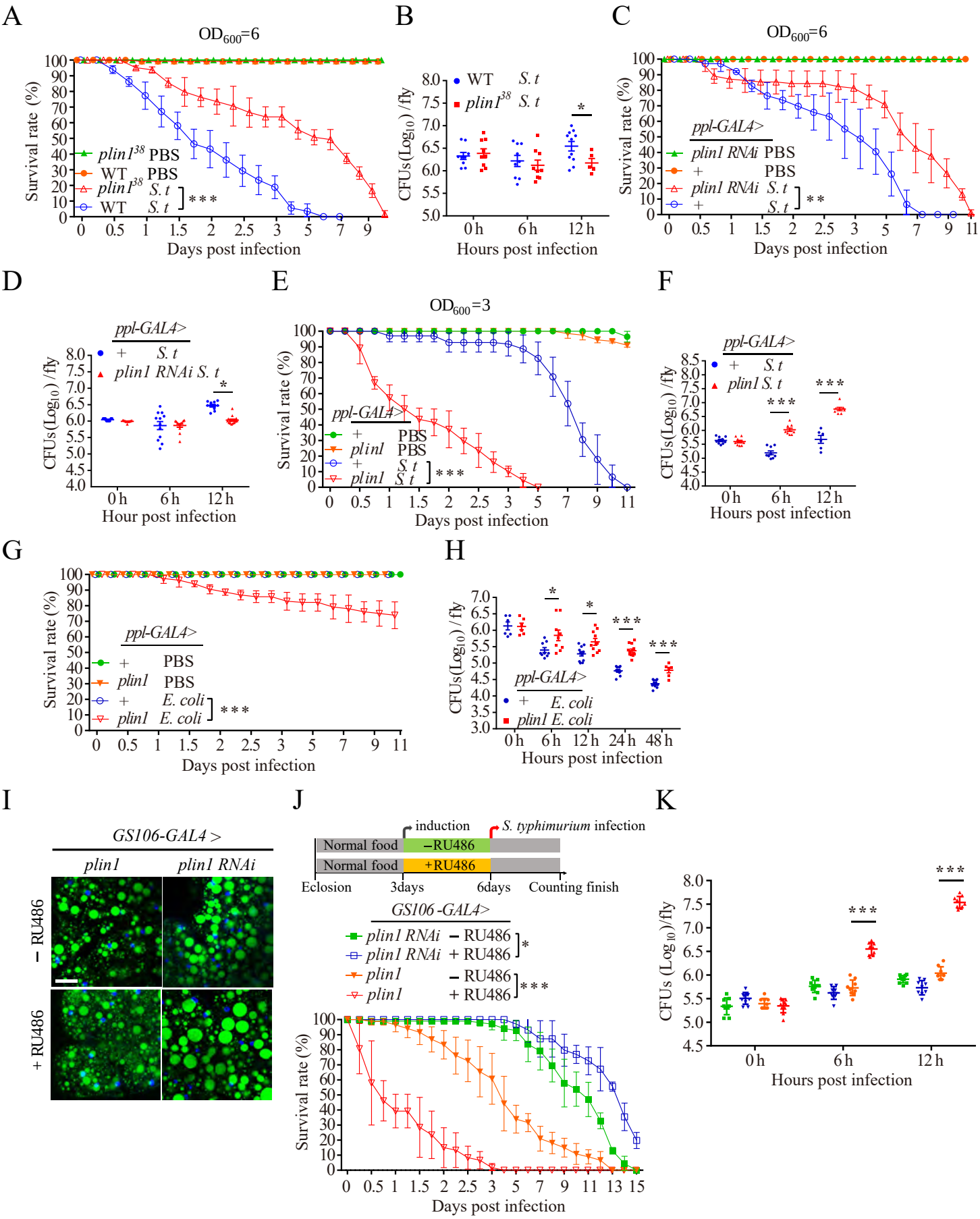
A
OD600=6
Survival rate (%)
plin1 38 PBS
WT PBS
plin1 38 S. t
WT S. t
***
Days post infection
B
CFUs(Log10) /fly
WT S. t
plin1 38 S. t
*
0 h
6 h
12 h
Hours post infection
C
OD600=6
Survival rate (%)
ppl-GAL4>
plin1 RNAi PBS
+ PBS
plin1 RNAi S. t
+ S. t
**
Days post infection
D
ppl-GAL4>
+ S. t
plin1 RNAi S. t
*
CFUs(Log10) /fly
0 h
6 h
12 h
Hour post infection
E
OD600=3
Survival rate (%)
ppl-GAL4>
+ PBS
plin1 PBS
+ S. t
plin1 S. t
***
Days post infection
F
ppl-GAL4>
+ S. t
plin1 S. t
***
***
CFUs(Log10) /fly
0 h
6 h
12 h
Hours post infection
G
Survival rate (%)
ppl-GAL4>
+ PBS
plin1 PBS
+ E. coli
plin1 E. coli
***
Days post infection
H
CFUs(Log10) / fly
*
*
***
***
ppl-GAL4>
+ E. coli
plin1 E. coli
0 h
6 h
12 h
24 h
48 h
Hours post infection
I
GS106-GAL4 >
plin1
plin1 RNAi
– RU486
+ RU486
J
induction
S. typhimurium infection
Normal food
–RU486
Normal food
+RU486
Eclosion
3days
6days
Counting finish
GS106 -GAL4>
plin1 RNAi – RU486
plin1 RNAi + RU486
*
plin1 – RU486
plin1 + RU486
***
Survival rate (%)
Days post infection
K
CFUs (Log10)/fly
***
***
0 h
6 h
12 h
Hours post infection

Fig. 4. *plin1* participates in the susceptibility of flies to bacterial infection. (**A** and **B**) Survival curves (**A**) and bacterial loads (CFUs) (**B**) of wild type and *plin1*^{38} flies (n =60) post *S. typhimurium* infection. (**C** and **D**) Survival curves (**C**) and bacterial loads (CFUs) (**D**) of *ppl-GAL4>plin1 RNAi* and control flies (n =60) post *S. typhimurium* infection. (**E** and **F**) Survival curves (**E**) and bacterial loads (CFUs) (**F**) of *ppl-GAL4>plin1* and control flies (n =60) post *S. typhimurium* infection. (**G** and **H**) Survival curves (**G**) and bacterial loads (CFUs) (**H**) of *ppl-GAL4>plin1* and control flies (n =60) post *E. coli* infection. (**I**) BODIPY staining (green) of LDs in the fat body of *GS106-GAL4>plin1* and *GS106-GAL4>plin1 RNAi* flies after 3 days with (lower panel) or without (upper panel) RU486 treatment. Eight fat bodies were examined for each sample. Scale bar: 20 μm. (**J** and **K**) Survival curves (**J**) and bacterial loads (CFUs) (**K**) of above flies (*I*) (n =60) post *S. typhimurium* infection. Values of plotted curves represent mean ± s.d. (**A, C, E, G, J**) of at least three independent repeats. Each scattering dot (CFUs) represents one technical replicate, line represents the mean of four independent repeats (**B, D, F, H, K**). Data were analyzed by Kaplan–Meier (**A, C, E, G, J**) and Multiple t-tests (**B, D, F, H, K**). *$p < 0.05$; ** $p < 0.01$; *** $p < 0.001$. **See also in Supplementary Figure 5.**

Figure 5

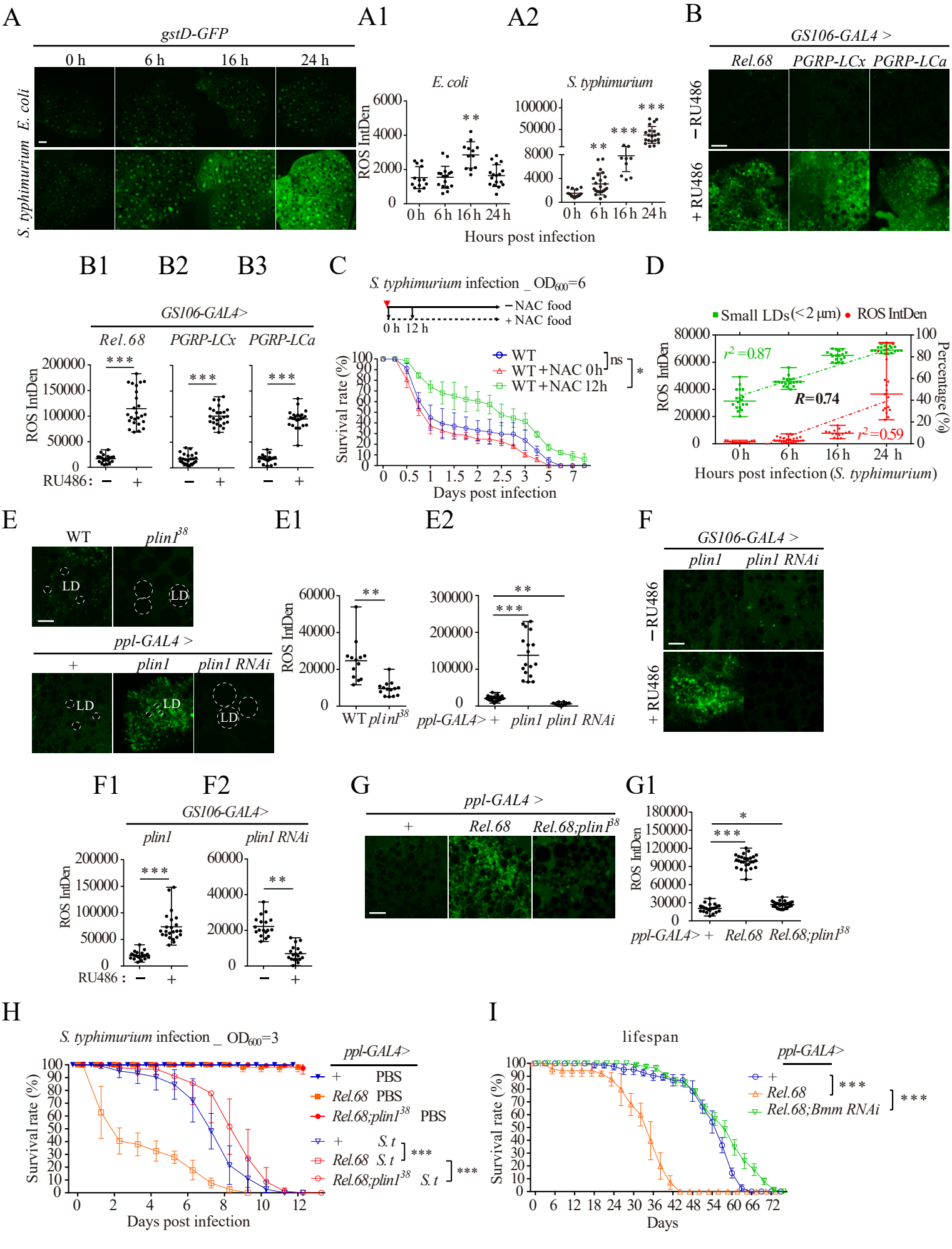
A
gstD-GFP
0 h
6 h
16 h
24 h
E. coli
S. typhimurium
A1
A2
E. coli
S. typhimurium
ROS IntDen
Hours post infection
B
GS106-GAL4 >
Rel.68
PGRP-LCx
PGRP-LCa
− RU486
+ RU486
B1
B2
B3
GS106-GAL4>
Rel.68
PGRP-LCx
PGRP-LCa
ROS IntDen
RU486:
C
S. typhimurium infection _ OD600=6
− NAC food
+ NAC food
0 h 12 h
WT
WT + NAC 0h
WT + NAC 12h
ns
Survival rate (%)
Days post infection
D
Small LDs (< 2 μm)
ROS IntDen
r2 =0.87
R=0.74
r2 =0.59
Percentage (%)
Hours post infection (S. typhimurium)
E
WT
plin1 38
LD
ppl-GAL4 >
+
plin1
plin1 RNAi
E1
E2
ROS IntDen
WT
plin1 38
ppl-GAL4> +
plin1
plin1 RNAi
F
GS106-GAL4 >
plin1
plin1 RNAi
− RU486
+ RU486
F1
F2
GS106-GAL4>
plin1
plin1 RNAi
ROS IntDen
RU486 :
G
ppl-GAL4 >
+
Rel.68
Rel.68;plin1 38
G1
ROS IntDen
ppl-GAL4> +
Rel.68
Rel.68;plin1 38
H
S. typhimurium infection _ OD600=3
ppl-GAL4>
+ PBS
Rel.68 PBS
Rel.68;plin1 38 PBS
+ S. t
Rel.68 S. t
Rel.68;plin1 38 S. t
Survival rate (%)
Days post infection
I
lifespan
ppl-GAL4>
+
Rel.68
Rel.68;Bmm RNAi
Survival rate (%)
Days

Fig. 5. The formation of large LDs ameliorates sustained inflammation induced oxidative stress. (**A**) ROS level indicated by GFP intensity (green) of *gstD-GFP* reporter in the fat body of wild type flies infected with *E. coli* (upper panel) or *S. typhimurium* (lower panel) at indicated time points. The statistics of GFP intensity was plotted in (**A1**) for *E. coli* infection and in (**A2**) for *S. typhimurium* infection. Eight fat bodies were examined for each sample and each scattering dot represents the data from one image. Scale bar: 20 μm. (**B**) ROS level indicated by DCFH-DA staining (green) in the fat body of indicated flies with (lower panel) or without (Upper panel) RU486 treatment for 5 days. The statistics of fluorescence intensity was plotted in (**B1**) for *GS106-GAL4>Rel.68* flies, in (**B2**) for *GS106-GAL4>PGRP-LCx* flies and in (**B3**) for *GS106-GAL4>PGRP-LCa* flies. Eight fat bodies were examined for each sample and each scattering dot represents the data from one image. Scale bar: 20 μm. (**C**) Survival curves of wild type flies (n=60 flies) with or without NAC treatment at indicated time post *S. typhimurium* infection. (**D**) Correlation analysis between the percentage of small LDs (< 2 μm, green) and intracellular ROS level (red) in fat body cells at indicated time points post *S. typhimurium* infection. The regression analysis was performed, respectively. Red regression dash line presents the change of intracellular ROS level (r^2 = 0.59) and green regression dash line present the change of small LDs percentage (r^2 = 0.87). The Pearson's correlation of these two set of data was analyzed (Pearson's correlation coefficient R=0.74). (**E**) ROS level indicated by DCFH-DA staining (green) in the fat body of indicated flies. The statistics of fluorescence intensity was plotted in (**E1**) for *plin1*^{38} and in (**E2**) for *ppl-GAL4>plin1* and *ppl-GAL4>plin1-RNAi* flies and their genetic controls, respectively. Dashed circle indicated LDs. Eight fat bodies were examined for each sample and each scattering dot represents the data from one image. Scale bar: 20 μm. (**F**) ROS level indicated by DCFH-DA staining (green) in the fat body of indicated flies with (lower panel) or without (upper panel) RU486 treatment for 5 days. The statistics of fluorescence intensity was plotted in (**F1**) for *GS106-GAL4>plin1* and in (**F2**) for *GS106-GAL4>plin1 RNAi* flies. Eight fat bodies were examined for each sample and each scattering dot represents the data from one image. Scale bar: 20 μm. (**G**) ROS level indicated by DCFH-DA staining (green) in the fat body of *ppl-GAL4>Rel.68*， *ppl-GAL4>Rel.68, plin*^{38} flies and control flies. The corresponding fluorescence intensity was quantified in (**G1**). Eight fat bodies were examined for each sample and each scattering dot represents the data from one image. Scale bar: 20 μm. (**H**) Survival curves of *ppl-GAL4>Rel.68*, *ppl-GAL4>Rel.68,plin*^{38} one-week old adult flies and control flies (n =60) after *S. typhimurium* infection. PBS injection as a control. (**I**) The lifespan curves of indicated flies at normal condition (n =60 per genotype). Error bars represent the mean with range (**A1-2, B1-3, C, E1-2, F1-2, G1**). Values of plotted curves represent mean ± s.d. of at least three independent repeats (**C, H, I**). Data was analyzed by One-Way ANOVA with Tukey's multiple-comparison test (**A1-2, E2, G1**), Student's t test (**B1-3, E1-2, F1-2**) and Kaplan–Meier (**C, H, I**). $^{*}p < 0.05$; $^{**}p < 0.01$; $^{***}p < 0.001$.

Figure 6

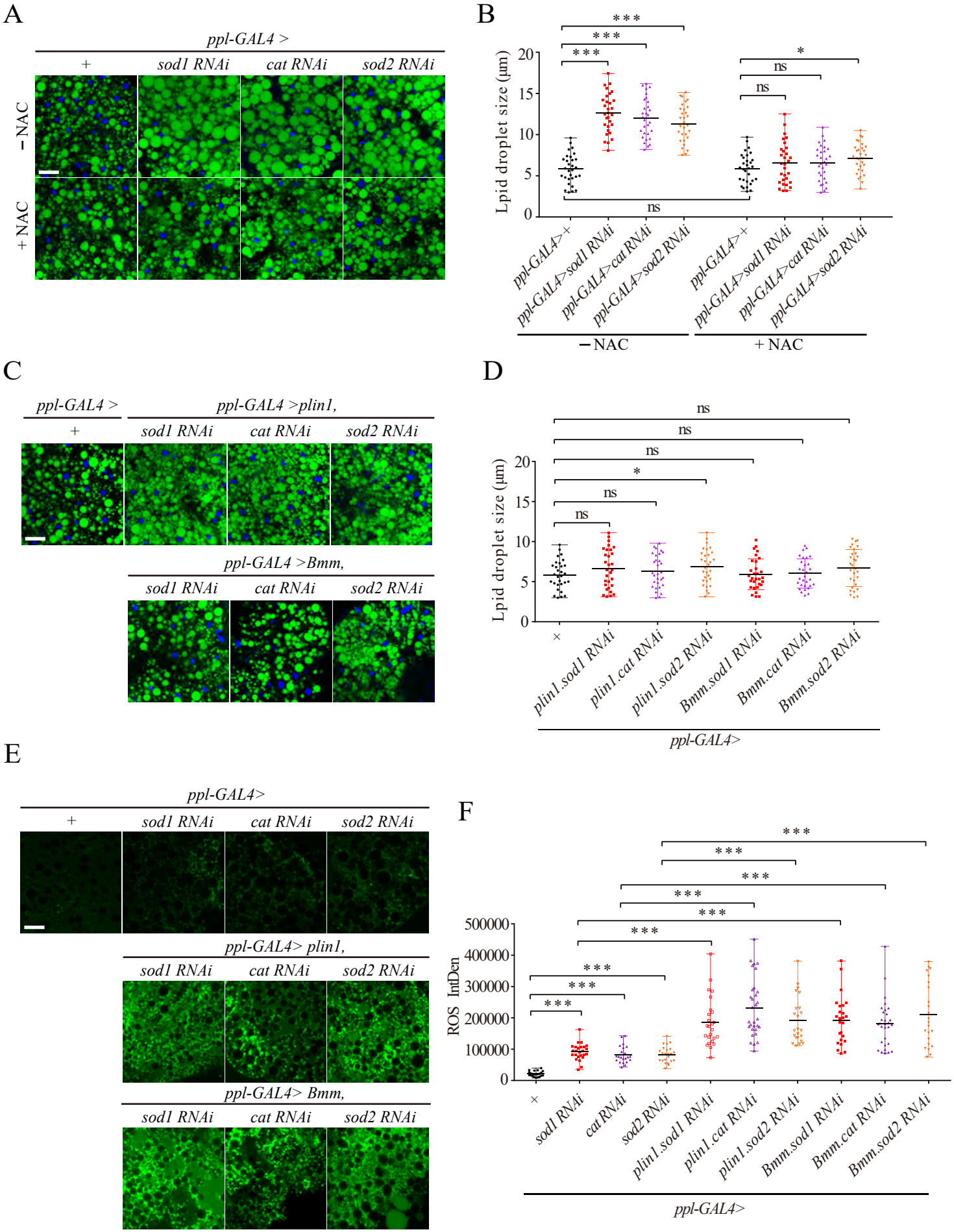
A
ppl-GAL4 >
+
sod1 RNAi
cat RNAi
sod2 RNAi
− NAC
+ NAC
B
Lpid droplet size (μm)
ppl-GAL4>+
ppl-GAL4>sod1 RNAi
ppl-GAL4>cat RNAi
ppl-GAL4>sod2 RNAi
− NAC
+ NAC
C
ppl-GAL4 >
ppl-GAL4 >plin1,
ppl-GAL4 >Bmm,
D
Lpid droplet size (μm)
plin1.sod1 RNAi
plin1.cat RNAi
plin1.sod2 RNAi
Bmm.sod1 RNAi
Bmm.cat RNAi
Bmm.sod2 RNAi
ppl-GAL4>
E
ppl-GAL4>
ppl-GAL4> plin1,
ppl-GAL4> Bmm,
F
ROS IntDen
ppl-GAL4>

Fig. 6. Adaptive large LDs formation contributes to eliminate excessive intracellular ROS. (**A** and **B**) BODIPY staining (green) of LDs (**A**) and the corresponding statistics of LDs' size (n =30 cells) (**B**) in the fat body of indicated flies after 5 days with (lower panel) or without (upper panel) N-acetyl-L-cysteine (NAC) treatment. Eight fat bodies were examined for each sample. Scale bar: 20 μm. (**C** and **D**) BODIPY staining (green) of LDs (**C**) and the corresponding statistics of LDs' size (n =30 cells) (**D**) in the fat body of indicated one-week old adult flies. Eight fat bodies were examined for each sample. Scale bar: 20 μm. (**E** and **F**) ROS levels indicated by DCFH-DA staining (green) in the fat body of indicated one-week old adult flies and control flies (**E**). The corresponding fluorescence intensity was quantified in (**F**). Eight fat bodies were examined for each sample and each scattering dot represents the data from one image. Scale bar: 20 μm. Error bars represent the mean with range. Data was analyzed by One-Way ANOVA with Tukey's multiple-comparison test (**B, D, F**) and Student's t test (**B, F**). *$p < 0.05$; ***$p < 0.001$; ns, no significance.

Figure 7

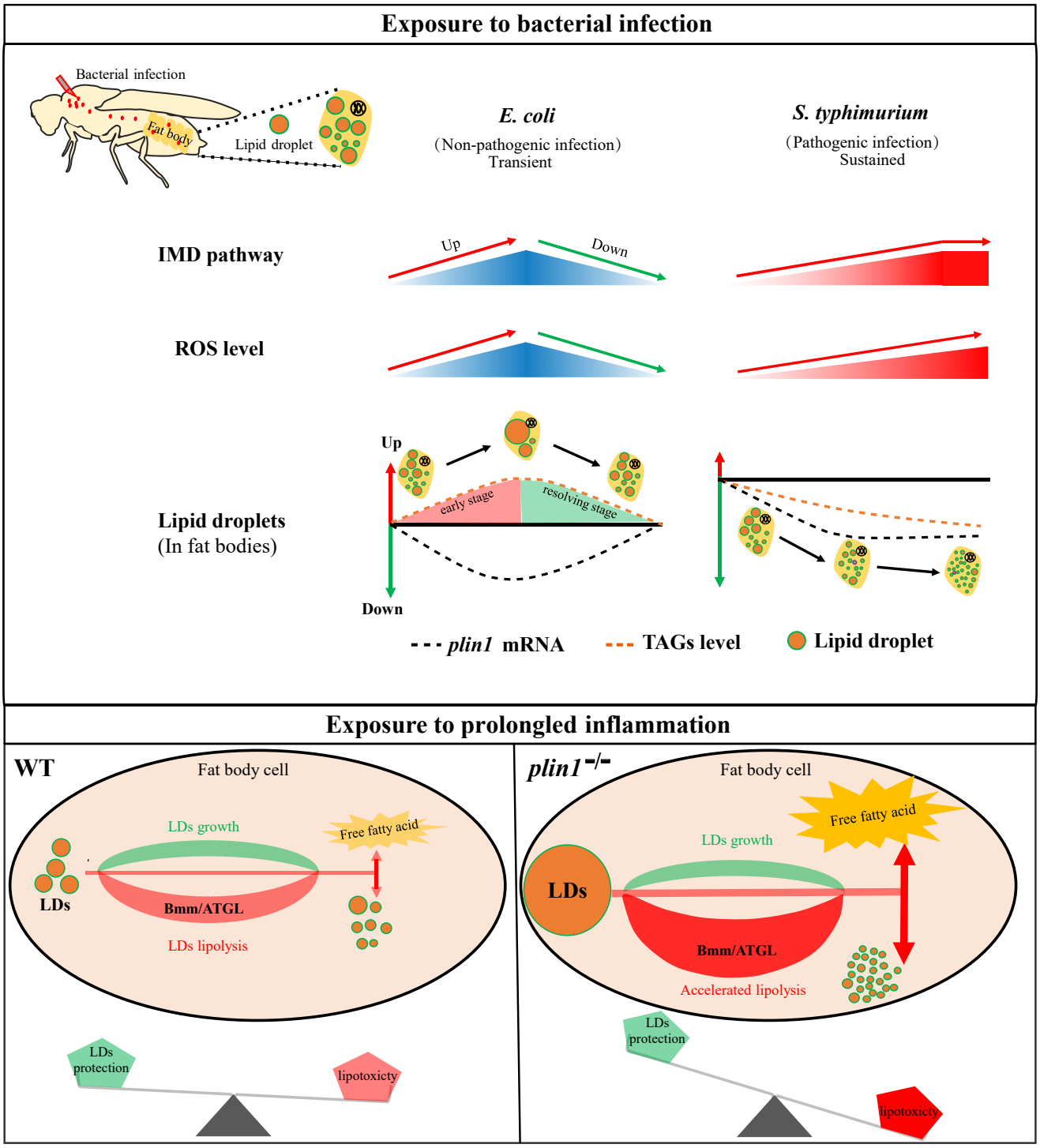
Exposure to bacterial infection
Bacterial infection
Fat body
Lipid droplet
E. coli
(Non-pathogenic infection)
Transient
S. typhimurium
(Pathogenic infection)
Sustained
IMD pathway
Up
Down
ROS level
Lipid droplets
(In fat bodies)
Up
Down
early stage
resolving stage
plin1 mRNA
TAGs level
Lipid droplet
Exposure to prolongled inflammation
WT
Fat body cell
LDs growth
Free fatty acid
LDs
Bmm/ATGL
LDs lipolysis
LDs protection
lipotoxicity
plin1 -/-
Fat body cell
Free fatty acid
LDs growth
LDs
Bmm/ATGL
Accelerated lipolysis
LDs protection
lipotoxicity

Fig. 7. The schematic diagram of LDs' morphogenesis mediated by Plin1 during infection-induced pathogenesis. LD's growth induced by downregulation of *plin1* at early-stage of *E. coli* infection. And enlarged LDs provides antioxidant role and benefits the host for anti-infection. While, sustained hyper-inflammation induced either by *S. typhimurium* infection or genetic manipulation triggers progressively enhanced LDs' lipolysis. And *plin1* deficiency accelerates excessive decomposition of large LDs, which results in energy wasting and severe lipotoxicity, thus deteriorated pathogenesis.

SUPPLEMENTAL INFORMATION

Supplemental Information includes five figures, and one table.

Supplementary Figure Legends

Figure S1

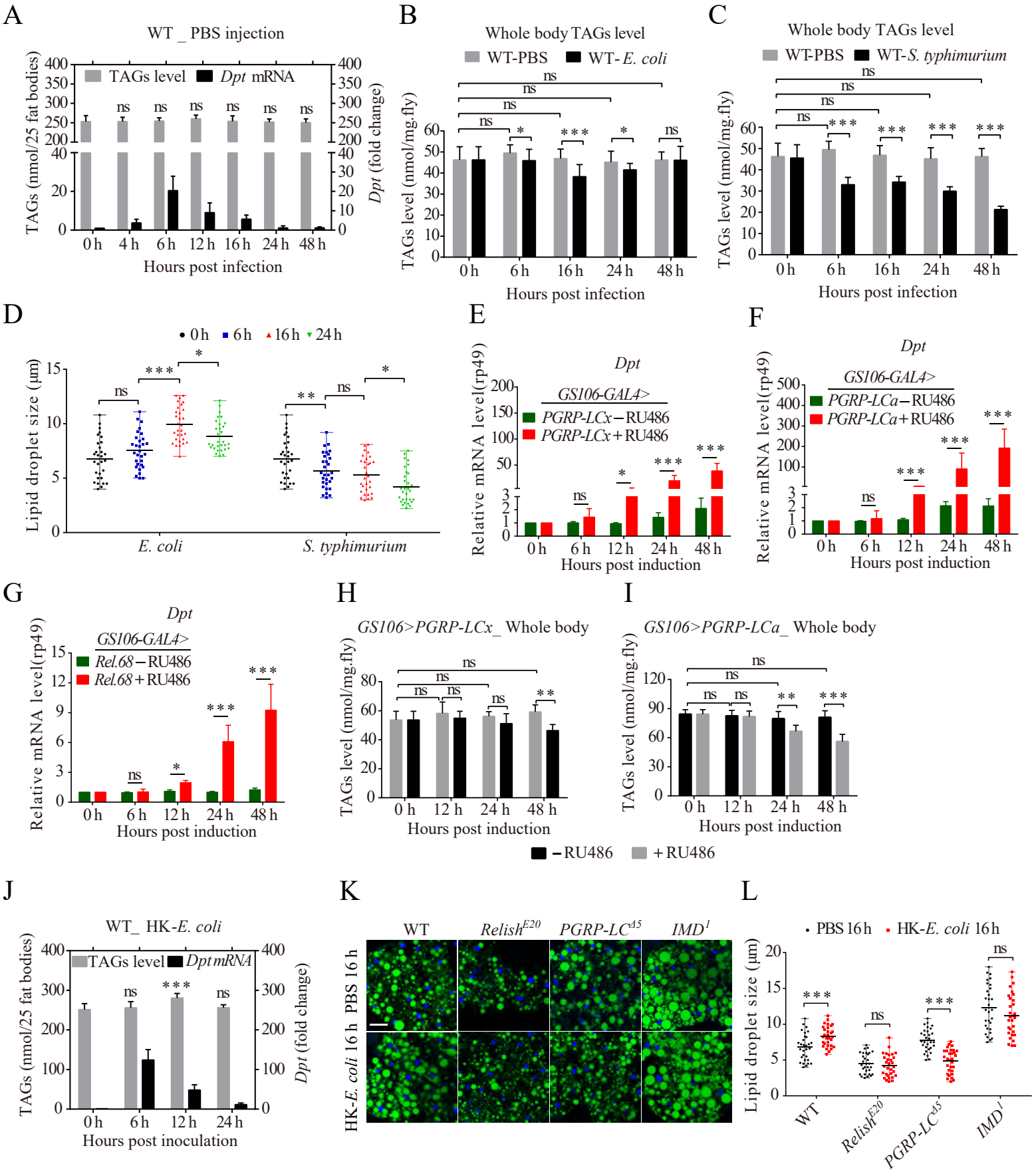
A
WT _ PBS injection
TAGs level
Dpt mRNA
TAGs (nmol/25 fat bodies)
Dpt (fold change)
0 h
4 h
6 h
12 h
16 h
24 h
48 h
Hours post infection
B
Whole body TAGs level
WT-PBS
WT-E. coli
TAGs level (nmol/mg.fly)
Hours post infection
C
Whole body TAGs level
WT-PBS
WT-S. typhimurium
TAGs level (nmol/mg.fly)
Hours post infection
D
0 h
6 h
16 h
24 h
Lipid droplet size (μm)
E. coli
S. typhimurium
E
Dpt
GS106-GAL4>
PGRP-LCx−RU486
PGRP-LCx+RU486
Relative mRNA level(rp49)
Hours post induction
F
Dpt
GS106-GAL4>
PGRP-LCa−RU486
PGRP-LCa+RU486
Relative mRNA level(rp49)
Hours post induction
G
Dpt
GS106-GAL4>
Rel.68−RU486
Rel.68+RU486
Relative mRNA level(rp49)
Hours post induction
H
GS106>PGRP-LCx_ Whole body
TAGs level (nmol/mg.fly)
Hours post induction
I
GS106>PGRP-LCa_ Whole body
TAGs level (nmol/mg.fly)
Hours post induction
−RU486
+RU486
J
WT_ HK-E. coli
TAGs level
Dpt mRNA
TAGs (nmol/25 fat bodies)
Dpt (fold change)
Hours post inoculation
K
WT
Relish^E20
PGRP-LC^Δ5
IMD^1
PBS 16 h
HK-E. coli 16 h
L
PBS 16 h
HK-E. coli 16 h
Lipid droplet size (μm)
WT
Relish^E20
PGRP-LC^Δ5
IMD^1

Fig. S1. IMD signaling modifies lipid metabolism and LDs morphology. Related to Figure 1. (**A**) Relative *Dptericin* (*Dpt*) mRNA expression (black) and TAGs level (gray) in the fat body of wild type flies at indicated time points after sterile PBS injection. The fold change of mRNA expression was normalized to that of 0 h and four independent repeats (n =20 flies per repeat) were performed at each time point. Total TAGs level of 25 flies' fat body tissues was quantified in six biological replicates at each time point. (**B** and **C**) Relative TAGs levels in the whole body of wild type flies at indicated time points post *E. coli* (**B**) or *S. typhimurium* (**C**) infection. Sterile PBS injection as a control. The change of TAG levels was normalized to that of 0 h, respectively. Six independent replicates for each time point were performed (n =12 flies per replicate). (**D**) The statistics of LDs' size (n =30 cells) in the fat body of wild type flies at indicated time point post *E. coli* or *S. typhimurium* infection. Each scattering dot represents the data from one fat body cell. (**E-G**) Relative *Dpt* mRNA expression in the fat body of *GS106-GAL4> PGRP-LCx* (**E**) and *GS106-GAL4> PGRP-LCa* (**F**) and *GS106-GAL4>Rel.68* (**G**) flies at indicated time point after with or without RU486 feeding. The data was normalized to that of 0 h without RU486 treatment. Four independent repeats at each time point were performed (n = 20 per repeat). (**H** and **I**) TAGs level in the whole body of *GS106-GAL4> PGRP-LCx* (**H**) and *GS106-GAL4> PGRP-LCa* (**I**) flies at indicated time point after with or without RU486 feeding. Six independent replicates for each time point were performed (n =12 flies in each replicate). (**J**) Relative *Dptericin* (*Dpt*) mRNA expression (black) and TAGs level (Grey) in the fat body of wild type flies at indicated time points post heat-killed *E. coli* (HK-*E. coli*) infection. The sample were treated and analyzed in the same way as above (**A**) described. (**K-L**) BODIPY staining (green) of LDs (**K**) and the corresponding statistics of LDs' size (n =30 cells) (**L**) in the fat body of IMD pathway mutant flies and corresponding genetic control flies. Eight fat bodies were examined for each sample. Scale bar: 20 μm. Error bars represent mean ± s.d. (**A-C, E-J**) or mean with range (**D, L**). Data were analyzed by One-way ANOVA with Tukey's multiple-comparison test (**A-D, H-J**) and Multiple t-tests (**B-C, E-I, L**). *$p < 0.05$; ** $p < 0.01$;*** $p < 0.001$; ns, no significance.

Figure S2

A

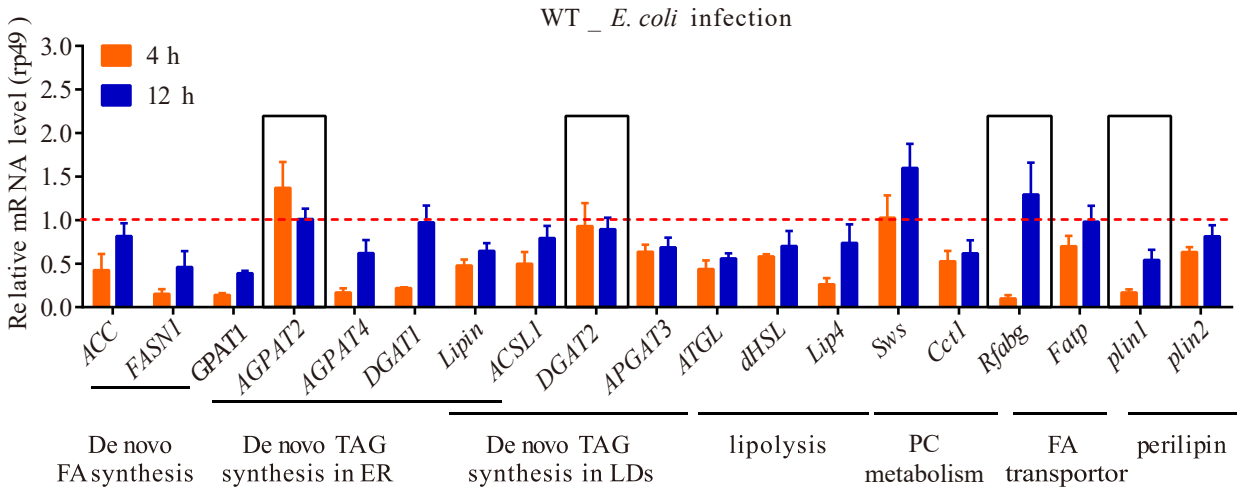

B

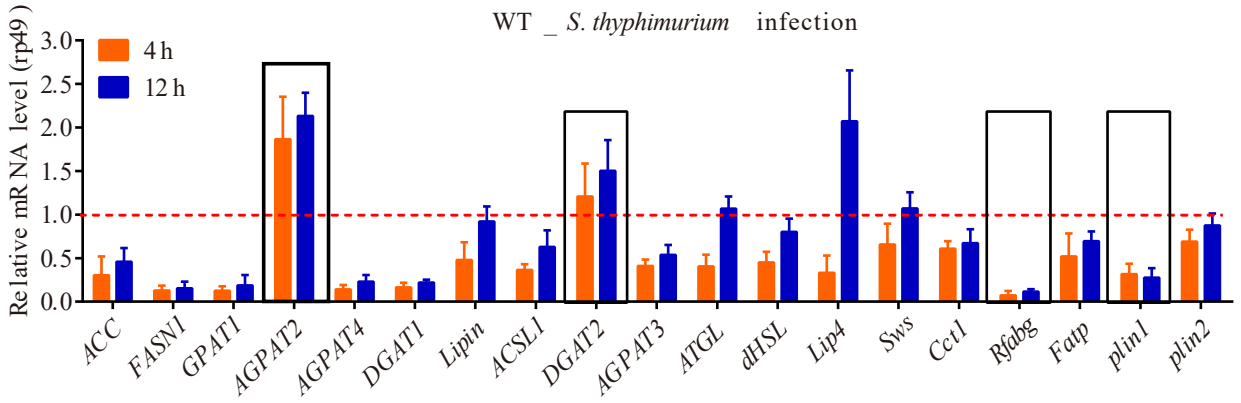

C

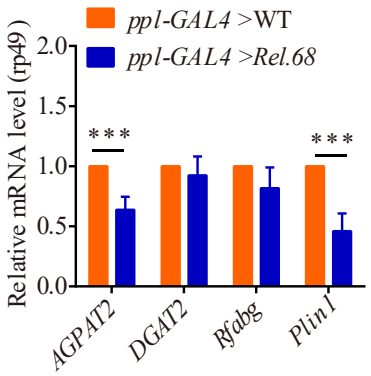

Fig. S2. The expression profile of genes involved in the regulation of LDs metabolism during IMD activation. Related to Figure 2. (**A** and **B**) Relative mRNA expression of a set of genes related to LD metabolism in the fat body of wild type flies at the indicated time points post *E. coli* (**A**) or *S. typhimurium* (**B**) infection. All measurements were normalized to that of 0 h (red line). Four independent repeats at each time point were performed (n = 20 per repeat). (**C**) Relative mRNA expression of genes *APGAT2*, *DGAT2*, *Rfabg* and *Plin1* in the fat body of *ppl-GAL4>Rel.68* flies compared with its genetic control flies of *ppl-GAL4> +*. Four independent repeats at each time point were performed (n = 20 per repeat). Error bars represent mean ± s.d.. Data were analyzed by Multiple t-tests. *** $p < 0.001$.

Figure S3

A

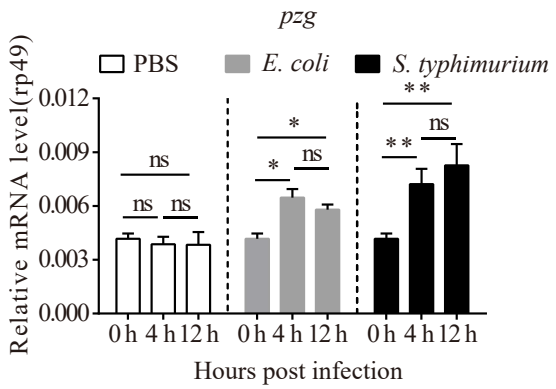

B

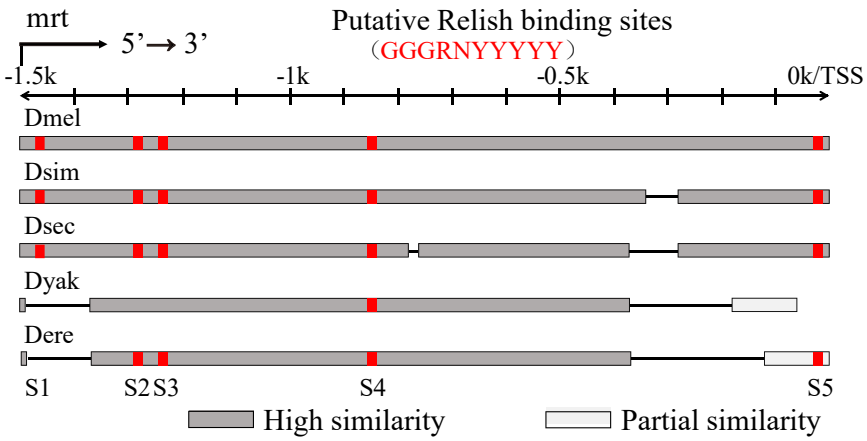

C

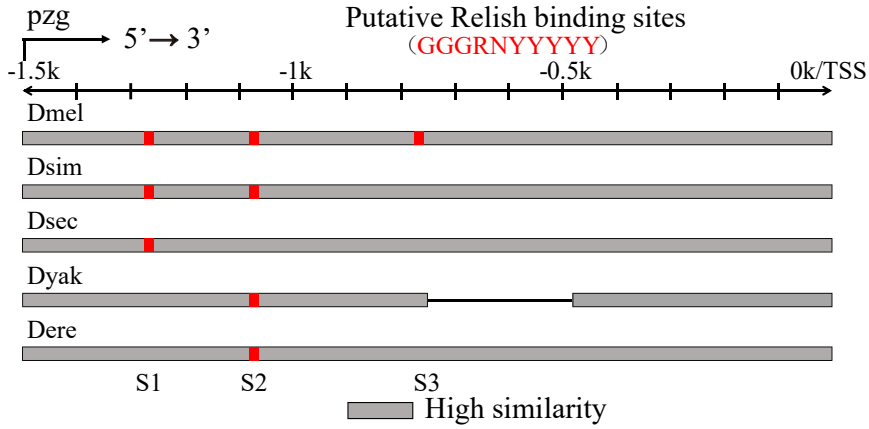

D

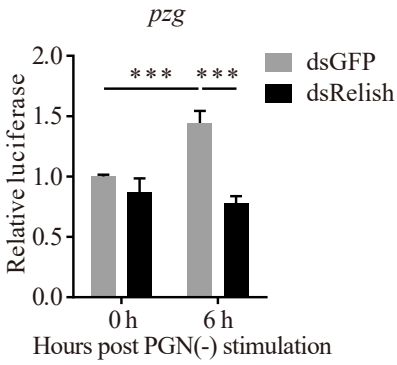

E

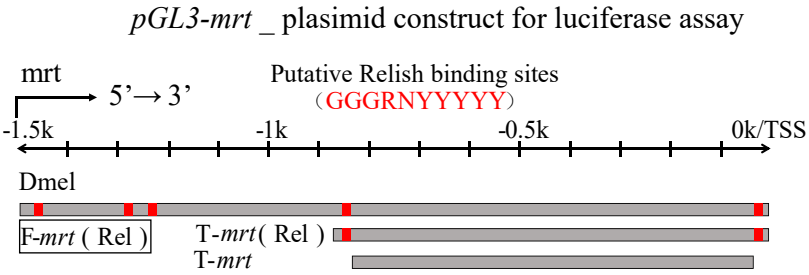

Fig. S3. Relish/NF-κB potentially regulates the transcription of *mrt* or *pzg* in *Drosophila* subgroups. Related to Figure 2. (**A**) Relative *pzg* mRNA levels in the fat body of wild type flies post *E. coli* or *S. typhimurium* infection. Flies treated with sterile PBS were used as a control. The fold change of mRNA expression was normalized to that of 0 h. Four independent repeats (n=20 flies fat body tissues per repeat) were performed at each time point for each group. (**B and C**) Predicted Relish/NF-κB-binding motifs in the promoter locus of *mrt* (**B**) and *pzg* (**C**) genes of five *Drosophila* subgroups. Dmel, *Drosophila melanogaster*; Dsim, *D. simulans*; sec, *D. sechelia*; Dyak, *D. yakuba*; Dere, *D. erecta*. S1-S5 represent the location site (red color) of conserved binding motifs. Sequence alignment is analyzed by BLAST in flybase website. TSS: transcription start site. (**D**) Relative luciferase activities of *pzg* (1.5 KB upstream of ATG, all predicted Relish binding sites are covered) reporter in S2* cells after double strand RNA (dsRNA) and PGN (35 μg/ml) treatment. All data were normalized to dsGFP control group at 0 h. Three independent repeats were performed at each time point for each treatment. (**E**) Schematic diagram of the *mrt* promoter locus and the plasmid constructs used for luciferase assay. The full length (F-*mrt*(Rel):-1.5k to +1bp), truncated length (T-*mrt*(Rel):-870 to +1bp) and mutant length (T-*mrt*:-870 to +1bp without binding motifs) of *mrt* promoter were indicated. Error bars represent the mean ± s.d.. Data were analyzed by One-way ANOVA with Tukey's multiple-comparison test (**A**) and Student's t test (**D**). $^*p < 0.05$; $^{**}p < 0.01$; $^{***}p < 0.001$; ns, no significance.

Figure S4

A

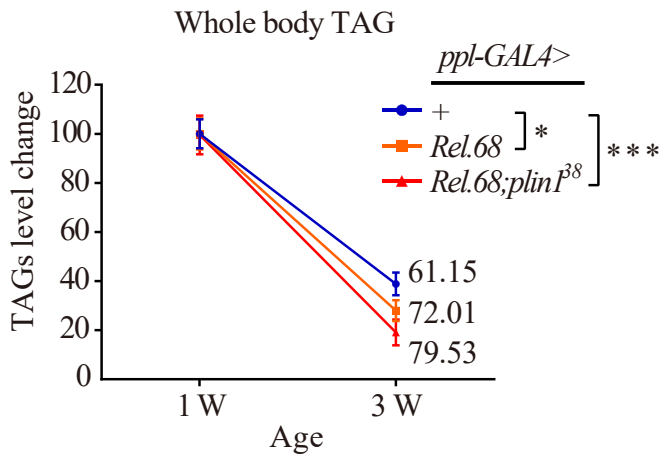
Whole body TAG
ppl-GAL4>
+
Rel.68
Rel.68;plinI38
*
***
TAGs level change
120
100
80
60
40
20
0
61.15
72.01
79.53
1 W
3 W
Age

B

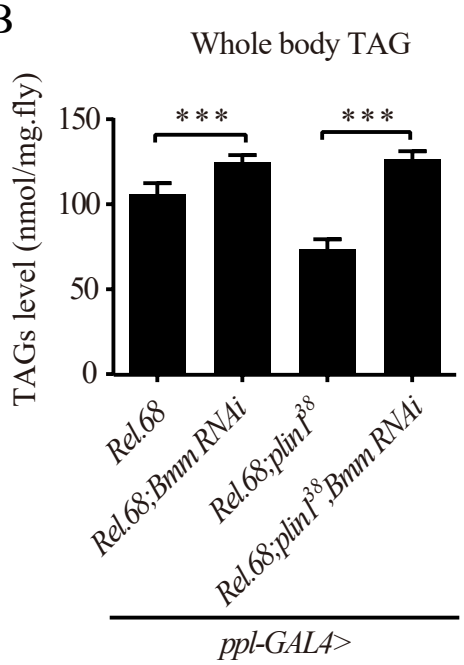
Whole body TAG
TAGs level (nmol/mg.fly)
150
100
50
0
***
***
Rel.68
Rel.68;Bmm RNAi
Rel.68;plinI38
Rel.68;plinI38,Bmm RNAi
ppl-GAL4>

Fig. S4. *plin1* deficiency enhances Bmm/ATGL-dependent lipolysis in the condition of sustained IMD activation. Related to Figure 3. (**A**) TAGs level change in the whole body of indicated one-week or three-week old flies. The change of TAG levels at 3 w was normalized to that of 1w for each genotype. The number on the right of each line represents the percentage reduction of TAGs level at 3 w compared with 1 w for each genotype. Six independent replicates at each time point for each genotype were performed (n =12 flies per replicate). (**B**) Relative TAGs levels in the whole body of indicated one-week old adult flies. All values of TAGs level were normalized to that of 0h of *ppl-GAL4*>+ control flies. Six independent replicates for each genotype were performed (n =12 flies per replicate). Error bars represent the mean ± s.d.. Data were analyzed by One-way ANOVA with Student t-test. $^{*}p < 0.05$; $^{***}p < 0.001$.

Figure S5

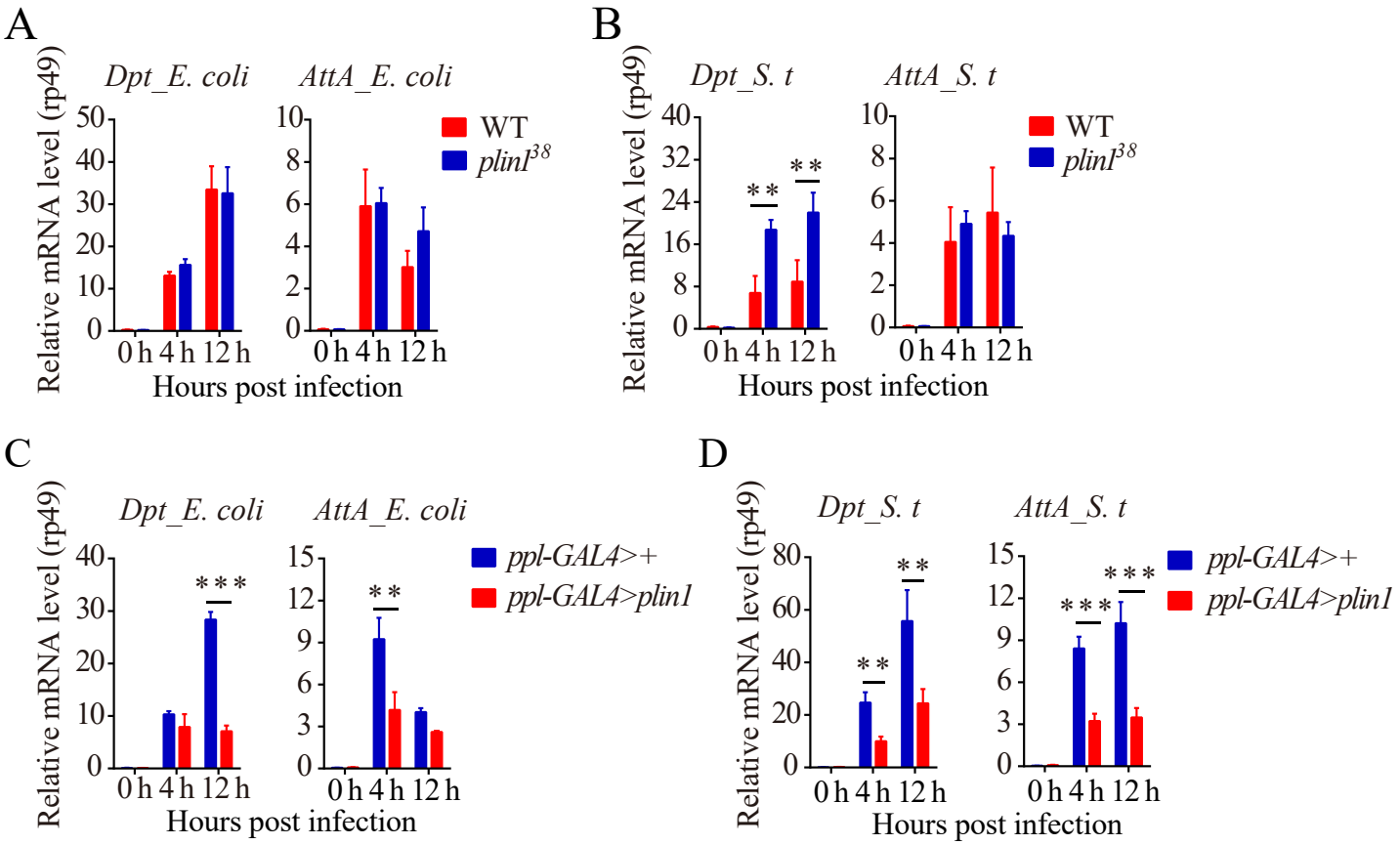
A
Dpt_E. coli
AttA_E. coli
Relative mRNA level (rp49)
WT
plinl38
0 h 4 h 12 h
Hours post infection
B
Dpt_S. t
AttA_S. t
C
ppl-GAL4>+
ppl-GAL4>plin1
D

Fig. S5. Overexpression *plin1* compromises AMP responses. Related to Figure 4. (**A** and **B**) Relative *diptericin (Dpt)* and *attacin-A (AttA)* mRNA expression in the fat body of *plin1*^{38} mutant flies and wild type flies at indicated time points post *E. coli* (**A**) or *S. typhimurium* (**B**) infection. Four independent repeats were performed (n = 20 per repeat). (**C** and **D**) Relative *diptericin (Dpt)* and *attacin-A (AttA)* mRNA expression of *ppl-GAL4> plin1* flies and *ppl-GAL4>* + control flies at indicated time points post *E. coli* (**C**) and *S. typhimurium* (**D**) infection. Four independent repeats were performed (n = 20 per repeat). Error bars represent mean ± s.d. Data was analyzed by Multiple t-tests. $^{**}p < 0.01$; $^{***}p < 0.001$.

1266 **Table S1: Primers used in this study.**

Genes	Forward primer	Reverse primer
	qRT-PCR primers	
Rp49	AGATCGTGAAGAAGCGCACCAAG	CACCAGGAACTTCTTGAATCCGG
Dpt	GGCTTATCCGATGCCCGACG	TCTGTAGGTGTAGGTGCTTCCC
AttA	CACAACTGGCGGAACTTTGG	AAACATCCTTCACTCCGGGC
plin1	CAGCGCATACCACTGGTCTAT	GCATTACCGATTTGCTTGACAG
plin2	CGAGCGCCTCCTTGAATAC	AGAACTCTTGCCATTCTGCAC
DGAT2/CG1942	GATTACTTTCCCGTGGAGCTGG	CCCATGTTAATGCCAATGCCTG
DGAT1/mdy	AAGACAGGCCTCTACTATTGT	CCCATCATGCCCATAAATGCC
DGAT/CG1941	GTTGCTGCCGTGCTGTTCTAT	GTGGGTTCTCTTGTGATTCGC
DGAT/CG1946	CTTCTTTACGCTGCCCATCTCG	CCATTACCTTCCATAATGCCG
GPAT1/CG5508	CCTTTTGGCCTTCACTTCC	TCTCGATCTGCTTCGTGTTC
APGAT4/CG4753	CTTCACATGCGGATTCTTCGTC	ACCATTCCGCCACACAGACAAG
APGAT3/CG4729	CTCTGTCCTGCATTTTCTACTACG	CTTGCTGATCTGCGTCTTGTTG
APGAT2/CG3812	GCTGGCCTAATCTTCATCG	CCCACAGTTTGATACGTTGC
APGAT1/CG17608	CTGTGCGTGCCCTTTATGATTC	CAGACCACGAACCTCCATTG
Lipin	GACATCCGCGATCTGTTTCCC	GGACTGGAATGTTTGGGTCAGC
Lip4	GACCGAACAAGGGACTTGG	CGAGTACGTATTGCCACGAA
ACC	GGAACACTGAACTGGGGAAA	GCAATCACGCTGGAGTTGTA
FASN	CGAATCCATCAATATGCCCG	ACATAGTGACCACCACCCAGGT
ACSL	TTCCGGCAAGATTATGCGTC	CAGTTGCTCCACAATTTGCTCA
dHSL	TTGCCCTCTTCAATGACAATCTG	CTGGTGGGTGTCCTTTCCA
BMM	AAGTATGCACCGCATCTGTTG	CAAATCGCAGAGGAGACAGC
sws/CG2212	CTGGATGGCGGCTATGTGAATAA	CCATTTCTTGTAGAGCAGCCAC
Cct1	TCCACCTCGCAGCAATTCTTC	GTAGTCACATCTATCCCGCTCC
Fatp	GAAATCCTTCTCGCGAATTCCT	GGAGATGAAAGCCATATCGCC
Rfabg	GGTTTCTGGCATATTGTTGA	TAGGGTGCGTATGCC ATCAA
DUOX	GCTGCACGCCAACCACAAGAGACT	CACGCGCAGCAGGATGTAAGGTTT
mrt	GGAGGATATTCTCGGAGTGGAGC	GCTTCCTGCCTCGTAGTCGAAC
pzg	GCTGAGGAACCACAACCATCTGAC	GTAACCTCGCCTTCGCCAGATT
	Primers for plasmid construction and dsRNA synthesis	
F-*mrt*(Rel)-luc	CGAGATCTGCGATCTAAGTATAACG TCGTAGCGCACACGCACACC	CAGTACCGGAATGCCAAGCTGGGT GCACCCTTTGATCAAGGTCTT
pzg-luc	CGAGATCTGCGATCTAAGTACACAG TAGCAGCACAACGGAGACG	CAGTACCGGAATGCCAAGCTCTGT AGCAGTTCTCGACGGACGCGT
T-*mrt*(Rel)-luc	CGAGATCTGCGATCTAAGTAGCCAC TTTGTCGCAGTGTATCTGT	CAACAGTACCGGAATGCCAGCTGG GTGCACCCTTTGATCAAG
T-*mrt*-luc	CGAGATCTGCGATCTAAGTACGTTA GCTTTTTGCTGTCATTCGT	CCAACAGTACCGGAATGCCAGATG CTGTTGGAAAACAAGCAA
dsRelish	TAATACGACTCACTATAGGGAGATC AAACACGTGCCGC	TAATACGACTCACTATACCCAGACT CACGCTCTGTCTC
dsGFP	TAATACGACTCACTATAGGGAGAAT GGTGAGCAAGGGCGAGGA	TAATACGACTCACTATAGGGAGACT TGTACAGCTCGTCCATGC

Supplementary Information for

Adaptive modification of lipid droplets mediated by Plin1 functions in infection-induced pathogenesis in *Drosophila*

Lei Wang[1,2,5], Jiaxin Lin[2,3,5], Junjing Yu[4], Zhiqin Fan[2,3], Hong Tang[2 #] and Lei Pan[2,3,6 #]

[1] Wuhan Institute of Virology, Chinese Academy of Sciences, Wuhan, Hubei 430071, China

[2] Key Laboratory of Molecular Virology and Immunology, Institut Pasteur of Shanghai, Chinese Academy of Sciences, Shanghai 200031, China

[3] CAS Center for Excellence in Biotic Interactions, University of Chinese Academy of Sciences, Beijing 100049, China

[4] Shanghai Institute of Biochemistry and Cell Biology, Chinese Academy of Sciences, Shanghai 200031, China.

[5] University of Chinese Academy of Sciences, Beijing 100049, China

[6] Lead contact

#Correspondence: H. Tang (htang@ips.ac.cn) or L. Pan (panlei@ips.ac.cn).

This PDF file includes:
SI Materials and Methods
Fig. S1 to S5 legend.
Table S1.

SI Materials and Methods.

Drosophila stocks and bacterial strain.

All flies were propagated at 25˚C on standard cornmeal food (1 L food contains 77.7 g cornmeal, 32.19 g yeast, 10.6 g agar, 0.726 g CaCl2, 31.62 g sucrose,63.2 g glucose, 2 g potassium sorbate and 15 ml 5% Tegosept),30%-55% humidity with a 12h/12h light/dark cycle. Fly resources that were used in this study as follows: w^{1118} were used as wild-type controls if no additional indication. *plin1*^{38}, *UAS-plin1* mcherry, *UAS-plin1 RNAi*, *Bmm-GFP* knock-in and *ppl-GAL4* were kindly gifted from Dr. Xun Huang (Institute of Genetics and Developmental Biology, CAS). *UAS-gstD-GFP* was kindly gifted from Dr. ZhiWei Liu (Shanghai Ocean University). w^{1118}*;P{GD5139=UAS-Bmm RNAi }*(VDRC, V37877 and V37880) were kindly gifted from Dr. Yong Liu (College of Life Sciences, Wuhan University). w^{1118}, *w[1118];P{w[+mW.hs]=Switch1}106*, *Bmm*^{1}, *w[*];P{w[+mC]=UAS-FLAG-Rel.68}i21-B; TM2/TM6C, Sb[1]*, *y[1] w[*]; P{w[+mC]=UAS-PGRP-LC.x}1* and *y[1] w[*]; P{w[+mC]=UAS-PGRP-LC.a}3* were obtained from Bloomington stock center. All flies used in this study were male. Two bacterial strain, *E. coli* (*DH5a*) and *S. typhimurium (SR-11)* (a gift from Dr. ZhiHua Liu, Institute of Biophysics, CAS) were used in this study.

Cloning and double-strand RNAs

To construct the *mrt* and *pzg* reporter vector (*mrt*-luc and *pzg*-luc), the *mrt* and *pzg* promoter sequence (about -1500 bp or -1000 bp to 0 bp) was PCR amplified from Drosophila genomic DNA and introduced into *pGL3* vector (Progema) at HindIII restriction site by using recombination technology (Hieff Clone® Plus One Step Cloning Kit, YEASEN). All the plasmid constructs were verified by nucleotide sequencing. *pAC5.1*-renilla plasmid as a normalized reporter. Double-stranded RNAs (dsRNAs) against relish or GFP used in the luciferase reporter assay were synthesized using MEGAscript T7 kit (Invitrogen). Primers used for PCR amplification are listed in Supplementary Table 1.

Infection and survival rate counting

Bacterial strains used in this study are *E. coli* (*DH5a*) and *Salmonella typhimurium* (*S. typhimurium*). Two days before infection, both bacteria from glycerol stocks were streaked onto Luria Broth (LB) agar plates and grown overnight at 37℃. The plate could be stored at 4 °C for up to 1 week. A single colony was inoculated to 6 ml fresh LB medium and grown at 37°C with shaking (200 rpm). Grow the bacteria to an OD600 of 0.7 to 0.8 (about 3.5 hours). The bacterial culture was pelleted with sterile phosphate-buffered saline (PBS) to the desired concentration. We injected 50.6 nl of bacterial suspension into dorsal prothorax of each fly with Nanoject II injector (Drummond). All flies used were 1 week old after eclosion. The final optical density (O.D. / ml) at 600 nm for injection were *E. coli* (O.D. 10) and *S. typhimurium* (O.D. 6 or O.D. 3). For *E.coli* infection, each fly obtained about 1x10^6 CFUs. For *S. typhimurium* infection, each fly obtained the lower dose (about 2x10^5 CFUs) or the higher dose (about 1x10^6 CFUs) according to the experiment design. Infected flies about 23 per vial were maintained at 25°C. Death was recorded at the indicated time point, and alive flies were

transferred to fresh food every day for the survival analysis and CFUs assay.

Lifespan counting

For lifespan analysis, male flies were collected within three days after adult emergence and raised in incubator (temperature: 25°C, humidity: 55%, 12:12 light: dark cycle). These flies were randomly divided into a separate vial in a number of 25 with at least three biological replicates. Dead flies were counted every three days and alive flies were flipped to fresh food.

Bacterial loads assay

To monitor bacterial loads of the flies during infection, the number of colony forming units (CFUs) grown on LB agar plate was determined as follow: 5 living flies were randomly collected in a 1.5 ml EP tube, rinsed with 70% ethanol two times by vertex for 10s to sterile the surface adherent bacteria, then rinsed with sterile deionized water two times by vertex for 10 s, and then homogenized in 200 μl of sterile PBS with three fly body volumes of ceramic beads (diameter: 0.5 mm) in the Minilys apparatus (Bertin TECHNOLOGIES) at highest speed for 30 s. The suspensions obtained were then serially diluted in PBS and plated on LB agar. Specially noted for S. typhimurium plating, PBS was substituted with PBS + 1% Triton X-100. For the bacterial load at zero time point, flies were allowed to rest for 10 min after bacterial injection before plating as described above. The agar plate was maintained at 37°C for 18 hours before CFUs counting. CFUs were $\log_{10}$ transformed.

Cell culture, transfection and luciferase assay

S2* cells (a gift from Dahua Chen, Institute of Zoology, CAS) were maintained in Drosophila Schneider's Medium (Invitrogen) supplemented with 10% heat-inactivated fetal bovine serum (Gibco), 100 units/ml of penicillin, and 100 mg/ml of streptomycin at 28°C. Transient transfection of various plasmids, dsRNA was performed with lipofectamine 3000 (Invitrogen), according to the manufacturer's manual. Luciferase reporter assays were carried out using a dual-luciferase reporter assay system (Promega). Where indicated, cells were treated with PGN (35 μg/μl, 6 h) purified from Erwinia carotovora carotovora 15 (*Ecc15*) referring to previous study(1).

qRT-PCR

For quantification of mRNA level, about 20 flies carcass/fat body tissue were dissected in sterile PBS buffer on ice at indicated time points post infection, immediately homogenized in 200 μl cold TRIzol with three fly body volumes of ceramic beads (diameter: 0.5 mm), then supplied additional 300 μl TRIzol to reach total 500 μl volume and samples were stored at -80°C.RNA extraction was referred to the manual of commercial kit (Magen, Hipure Total RAN Plus Micro Kit), this kit can effectively remove genomic DNA contamination. cDNA was synthesized by using the kit (abm, 5X All-In-One MasterMix) with total 1μg isolated RNA as template in a 20 μl reaction system. Quantitative real-time PCR (qRT-PCR) was performed using a SYBR green kit (abm, EvaGreen supermaster Mix) on an ABI 7500 or ViiATM 7 thermocycler (Life

Technology). Samples from at least four independent biological replicates per genotype were collected and analyzed. House-keeping gene rp49 as the reference gene for data normalization. Primer data for qRT-PCR are provided in Supplementary Table 1.

Lipid droplet staining and counting

For lipid droplet staining, adult male carcass/fat body tissues were dissected and fixed in 4% fresh prepared paraformaldehyde (PH=7.5) in PBS for 10 min on ice. Tissues were then rinsed twice with PBS (3 min each time), then incubated in PBS containing 1μg/ml of BODIPY 493/503(Invitrogen) dye or 0.5 μg/ml Nile Red (Sigma) for 30 min on ice, DAPI (1μg/μl, final concentration) was added to stain nuclei at last 5 mins of staining process. After staining, tissues were rinsed three times with PBS (3 mins each time), then mounted in mounting medium (Vector, H-1000) for microscopy analysis. To quantify the average lipid droplet size, the average diameter of the three largest lipid droplets per cell was measured generally, with the exception of *plin1* deficiency associated flies, we measured their biggest lipid droplets in one cell (2). 30 fat body cells of each genotype fly randomly selected from eight confocal images were used to analysis the lipid droplet size. To count the size distribution of lipid droplets, the average percentage of the indicated size range of lipid droplets per cell from 30 fat body cells were determined by using the "Analyze Particles" tool embedded in ImageJ software (https://imagej.nih.gov/ij/). To quantify the fluorescence intensity of GFP on the surface of lipid droplets, confocal images acquired from eight fat bodies were measured by ImageJ software.

TAG assay

TAG amounts were measured using a TG Quantification Kit (BIOSINO, TG kit). Briefly, for whole body TAG quantification, groups of 12 one-week old male flies were collected and weighted (about 10 mg) in a 1.5 ml EP tube, then immediately stored at -80°C for subsequent assay. Stored flies were homogenized in 200 μl lysis buffer (10mM KH_2PO4, 1mM EDTA, PH=7.4) with three fly body volumes of ceramic beads, and inactivated in water bath at 75°C for 15 min. The inactivated homogenate was homogenized again for 30 s and kept on ice ready for assay. For each TAG measurement, 3 μl of homogenate was incubated with 250 μl reaction buffer at 37°C for 10 min. After removal debris by centrifugation (2000 rpm, 2 min), 150 μl of clear supernatant was used to perform a colorimetric assay in 96 well plate (Corning® Costar) for absorbance reading at 505 nm. TAGs level was normalized with fly weight in each homogenate (unit: nmol/mg.fly). For fat body TAG quantification, 25 fly's carcass/fat body tissues were dissected and following assay as described above. TAGs level was normalized with per 25 flies (unit: nmol/25.fly).

RU486 treatment

RU486 induction was described as before (3). Briefly, A 10 mg/ml stock solution of RU486 (mifepristone; Sigma) was dissolved in DMSO. Appropriate volumes of RU486 stock solution was diluted with water containing 2% ethanol to final concentration of 50 μg/ml.100 μl of the diluted RU486 solution was dipped onto the surface of fresh

164 food in vials (Diameter: 2 cm). The vials were then allowed to dry at room temperature
165 for half day or 4℃ for overnight. Flies were transferred to RU486-contained food and
166 raised in 25℃ and fresh food was changed every two days.
167
168 **NAC Treatment**
169 N-acetyl-L-cysteine (NAC) (Beyotime) fresh solution was prepared by dissolving 0.5
170 g of NAC powder in 10 ml distilled water, the solution could be aliquoted into 1 ml per
171 EP tube and frozen or stored at -80 °C. 100 μl of NAC solution was dipped onto the
172 surface of fresh food in vials (Diameter: 2 cm). The vials were then allowed to dry at
173 room temperature for half day or 4℃ for overnight. Flies were transferred to NAC-
174 contained food and raised in 25℃ and fresh food was changed every day.
175
176 **ROS detection**
177 We used two methods to detect ROS in fat body, which are *gstD-GFP* reporter flies and
178 dichlorofluorescein diacetate (DCFH-DA) labeling. The oxidative stress reporter
179 construct *gstD-GFP* for evaluating cellular ROS levels has been describe before (4).
180 Briefly, the carcass/fat body of transgenic flies containing a *gstD-GFP* reporter
181 construct were dissected in sterile PBS, fixed in 4% formaldehyde for 10 min on ice,
182 rinsed twice with ice-chilled PBS (3 min each time), then the flaky fat body cells
183 attached to the inner carcass shell were dissected out to mount and confocal image
184 (Vector, H-1000). DCFH-DA (Beyotime, Reactive Oxygen Species Assay Kit) labeling
185 of fresh dissected carcass/fat body tissues was performed according to the
186 manufacturer's manual, which based on the ROS-dependent oxidation of DCFH-DA to
187 fluorescent molecule 2'-7'dichlorofluorescein (DCF). In brief, the tissues were
188 incubated with PBS containing 20 μM DCFH-DA for 30 min at 37℃, washed with
189 sterile PBS for three times (3 min each) to remove free DCFH-DA that do not uptake
190 by the cell, then the flaky fat body cells attached to the inner carcass shell immediately
191 were dissected out to mount and confocal image (Vector, H-1000). It should be noted
192 that the slices were confocal imaged using the exact same settings for control and
193 experimental groups. The fluorescence intensity is proportional to the ROS levels,
194 fluorescence intensity of GFP or DCF was quantified by using ImageJ software.
195
196 **Starvation test**
197 Adult male flies were collected within three days after eclosion and raised on standard
198 fly food at 25˚C. One week later, flies were randomly distributed in groups of 20
199 flies/vial and starved on 1% agar (dissolved in distilled water), new agar vial was
200 changed every day. For the survival counting, the deaths were scored every two hours
201 until all experimental files were dead. For the TAG assay, 12 alive flies were randomly
202 collected at indicated time point, and delivered to TAG assay as describe above.
203
204 **Microscopy and software**
205 LSM700 (Leica) and Olympus FV-1200 confocal laser scanning microscopy were used
206 for imaging. Captured images were analyzed by implemented soft respectively. ImageJ
207 (https://imagej.nih.gov/ij/) was used for analysis of fluorescence intensity and lipid

droplets size.

Statistical analyses

All replicates are showed as the mean ± SD or mean with range. Statistical significance was determined using a paired Student's t-test for two measurements, one-way ANOVA (Tukey's HSD) with a multiple t-tests and Multiple t-tests for pairwise comparisons. Kaplan–Meier test for survival curves comparison. All data processing was used with GraphPad Prism 7.0.

Sample size choice. The sample size was determined according to the number of data points. Batches of experiment were carried out to ensure repeatability and the use of enough animals for each data point.

Randomization. Measures were taken to ensure randomization. Each experimental batch contained more animals than the number of data points, to ensure randomization and the accidental exclusion of animals. In vitro analyses were usually performed on a specimen from animals at each data point to ensure a minimum of three biological replicates.

Blinding. Data collection and data analysis were routinely performed by different people to blind potential bias. All measurement data are expressed as mean ± s.d. to maximally show derivations, unless otherwise specified.

References for SI

1. Gottar M GV, Michel T, Belvin M, Duyk G, Hoffmann JA, Ferrandon D, Royet J. (2002) The Drosophila immune response against Gram-negative bacteria is mediated by a peptidoglycan recognition protein. *Nature* 11(416(6881)):640-644.
2. Bi J*, et al.* (2012) Opposite and redundant roles of the two Drosophila perilipins in lipid mobilization. *Journal of cell science* 125(Pt 15):3568-3577.
3. Poirier L SA, Zheng J, Seroude L. (2008) Characterization of the Drosophila gene-switch system in aging studies: a cautionary tale. *Aging Cell. 2008 Oct;* 7(5)(758-70.).
4. Sykiotis GP & Bohmann D (2008) Keap1/Nrf2 signaling regulates oxidative stress tolerance and lifespan in Drosophila. *Developmental cell* 14(1):76-85.

Supplementary Figure Legends

Fig. S1. IMD signaling modifies lipid metabolism and LDs morphology. Related to Figure 1. (**A**) Relative *Dptericin* (*Dpt*) mRNA expression (black) and TAGs level (gray) in the fat body of wild type flies at indicated time points after sterile PBS injection. The fold change of mRNA expression was normalized to that of 0 h and four independent repeats (n =20 flies per repeat) were performed at each time point. Total TAGs level of

252 25 flies' fat body tissues was quantified in six biological replicates at each time point.
253 (**B** and **C**) Relative TAGs levels in the whole body of wild type flies at indicated time
254 points post *E. coli* (**B**) or *S. typhimurium* (**C**) infection. Sterile PBS injection as a
255 control.The change of TAG levels was normalized to that of 0 h, respectively. Six
256 independent replicates for each time point were performed (n =12 flies per replicate).
257 (**D**) The statistics of LDs' size (n =30 cells) in the fat body of wild type flies at indicated
258 time point post *E. coli* or *S. typhimurium* infection. Each scattering dot represents the
259 data from one fat body cell. (**E-G**) Relative *Dpt* mRNA expression in the fat body of
260 *GS106-GAL4> PGRP-LCx* (**E**) and *GS106-GAL4> PGRP-LCa* (**F**) and *GS106-*
261 *GAL4>Rel.68* (**G**) flies at indicated time point after with or without RU486 feeding.
262 The data was normalized to that of 0 h without RU486 treatment. Four independent
263 repeats at each time point were performed (n = 20 per repeat). (**H** and **I**) TAGs level in
264 the whole body of *GS106-GAL4> PGRP-LCx* (**H**) and *GS106-GAL4> PGRP-LCa* (**I**)
265 flies at indicated time point after with or without RU486 feeding. Six independent
266 replicates for each time point were performed (n =12 flies in each replicate). (**J**)
267 Relative *Dptericin* (*Dpt*) mRNA expression (black) and TAGs level (black) in the fat
268 body of wild type flies at indicated time points post heat-killed *E. coli* (HK-*E. coli*)
269 infection. The sample were treated and analyzed in the same way as above (**A**)
270 described. (**K-L**) BODIPY staining (green) of LDs (**K**) and the corresponding statistics
271 of LDs' size (n =30 cells) (**L**) in the fat body of IMD pathway mutant flies and
272 corresponding genetic control flies. Eight fat bodies were examined for each sample.
273 Scale bar: 20 μm. Error bars represent mean ± s.d. (**A-C, E-J**) or mean with range (**D,**
274 **L**). Data were analyzed by One-way ANOVA with Tukey's multiple-comparison test
275 (**A-D, H-J**) and Multiple t-tests (**B-C, E-I, L**). *$p < 0.05$; *** $p < 0.001$; ns, no
276 significance.
277
278 **Fig. S2.** The expression profile of genes involved in the regulation of LDs metabolism
279 during IMD activation. Related to Figure 2. (**A** and **B**) Relative mRNA expression of a
280 set of genes related to LD metabolism in the fat body of wild type flies at the indicated
281 time points post *E. coli* (**A**) or *S. typhimurium* (**B**) infection. All measurements were
282 normalized to that of 0 h (red line). Four independent repeats at each time point were
283 performed (n = 20 per repeat). (**C**) Relative mRNA expression of genes *APGAT2*,
284 *DGAT2*, *Rfabg* and *Plin1* in the fat body of *ppl-GAL4>Rel.68* flies compared with its
285 genetic control flies of *ppl-GAL4> +*. Four independent repeats at each time point were
286 performed (n = 20 per repeat). Error bars represent mean ± s.d.. Data were analyzed by
287 Multiple t-tests. *** $p < 0.001$.
288
289 **Fig. S3.** Relish/NF-κB potentially regulates the transcription of *mrt* or *pzg* in
290 *Drosophila* subgroups. Related to Figure 2. (**A**) Relative *pzg* mRNA levels in the fat
291 body of wild type flies post *E. coli* or *S. typhimurium* infection. Flies treated with sterile
292 PBS were used as a control. The fold change of mRNA expression was normalized to
293 that of 0 h. Four independent repeats (n=20 flies fat body tissues per repeat) were
294 performed at each time point for each group. (**B and C**) Predicted Relish/NF-κB-
295 binding motifs in the promoter locus of *mrt* (**B**) and *pzg* (**C**) genes of five *Drosophila*

subgroups. Dmel, *Drosophila melanogaster*; Dsim, *D. simulans*; sec, *D. sechelia*; Dyak, *D. yakuba*; Dere, *D. erecta*. S1-S5 represent the location site (red color) of conserved binding motifs. Sequence alignment is analyzed by BLAST in flybase website. TSS: transcription start site. (**D**) Relative luciferase activities of *pzg* (1.5 KB upstream of ATG, all predicted Relish binding sites are covered) reporter in S2* cells after double strand RNA (dsRNA) and PGN (35 μg/ml) treatment. All data were normalized to dsGFP control group at 0 h. Three independent repeats were performed at each time point for each treatment. (**E**) Schematic diagram of the *mrt* promoter locus and the plasmid constructs used for luciferase assay. The full length (F-*mrt*(RelB):-1.5k to +1bp), truncated length (T-*mrt*(RelB):-870 to +1bp) and mutant length (T-*mrt*:-870 to +1bp without binding motifs) of *mrt* promoter were indicated. Error bars represent the mean ± s.d.. Data were analyzed by One-way ANOVA with Tukey's multiple-comparison test (**A**) and Student's t test (**D**). $*p < 0.05$; $**p < 0.01$; $***p < 0.001$; ns, no significance.

Fig. S4. *plin1* deficiency enhances Bmm/ATGL-dependent lipolysis in the condition of sustained IMD activation. Related to Figure 3. (**A**) TAGs level change in the whole body of indicated one-week or three-week old flies. The change of TAG levels at 3 w was normalized to that of 1w for each genotype. The number on the right of each line represents the percentage reduction of TAGs level at 3 w compared with 1 w for each genotype. Six independent replicates at each time point for each genotype were performed (n =12 flies per replicate). (**B**) Relative TAGs levels in the whole body of indicated one-week old adult flies. All values of TAGs level were normalized to that of 0h of *ppl-GAL4>+* control flies. Six independent replicates for each genotype were performed (n =12 flies per replicate). Error bars represent the mean ± s.d.. Data were analyzed by One-way ANOVA with Student t-test. $*p < 0.05$; $***p < 0.001$.

Fig. S5. Overexpression *plin1* compromises AMP responses. Related to Figure 4. (**A** and **B**) Relative *diptericin (Dpt)* and *attacin-A (AttA)* mRNA expression in the fat body of $plin1^{38}$ mutant flies and wild type flies at indicated time points post *E. coli* (**A**) or *S. typhimurium* (**B**) infection. Four independent repeats were performed (n = 20 per repeat). (**C** and **D**) Relative *diptericin (Dpt)* and *attacin-A (AttA)* mRNA expression of *ppl-GAL4> plin1* flies and *ppl-GAL4>* + control flies at indicated time points post *E. coli* (**C**) and *S. typhimurium* (**D**) infection. Four independent repeats were performed (n = 20 per repeat). Error bars represent mean ± s.d. Data was analyzed by Multiple t-tests. $**p < 0.01$; $***p < 0.001$.

Table S1: Primers used in this study.

Genes	Forward primer	Reverse primer
	qRT-PCR primers	
Rp49	AGATCGTGAAGAAGCGCACCAAG	CACCAGGAACTTCTTGAATCCGG
Dpt	GGCTTATCCGATGCCCGACG	TCTGTAGGTGTAGGTGCTTCCC
AttA	CACAACTGGCGGAACTTTGG	AAACATCCTTCACTCCGGGC
plin1	CAGCGCATACCACTGGTCTAT	GCATTACCGATTTGCTTGACAG

plin2	CGAGCGCCTCCTTGAATAC	AGAACTCTTGCCATTCTGCAC
DGAT2/CG1942	GATTACTTTCCCGTGGAGCTGG	CCCATGTTAATGCCAATGCCTG
DGAT1/mdy	AAGACAGGCCTCTACTATTGT	CCCATCATGCCCATAAATGCC
DGAT/CG1941	GTTGCTGCCGTGCTGTTCTAT	GTGGGTTCTCTTGTGATTCGC
DGAT/CG1946	CTTCTTTACGCTGCCCATCTCG	CCATTACCTTCCATAATGCCG
GPAT1/CG5508	CCTTTTGGCCTTCACTTCC	TCTCGATCTGCTTCGTGTTC
APGAT4/CG4753	CTTCACATGCGGATTCTTCGTC	ACCATTCCGCCACACAGACAAG
APGAT3/CG4729	CTCTGTCCTGCATTTTCTACTACG	CTTGCTGATCTGCGTCTTGTTG
APGAT2/CG3812	GCTGGCCTAATCTTCATCG	CCCACAGTTTGATACGTTGC
APGAT1/CG17608	CTGTGCGTGCCCTTTATGATTC	CAGACCACGAACCTCCATTG
Lipin	GACATCCGCGATCTGTTTCCC	GGACTGGAATGTTTGGGTCAGC
Lip4	GACCGAACAAGGGACTTGG	CGAGTACGTATTGCCACGAA
ACC	GGAACACTGAACTGGGGAAA	GCAATCACGCTGGAGTTGTA
FASN	CGAATCCATCAATATGCCCG	ACATAGTGACCACCACCCAGGT
ACSL	TTCCGGCAAGATTATGCGTC	CAGTTGCTCCACAATTTGCTCA
dHSL	TTGCCCTCTTCAATGACAATCTG	CTGGTGGGTGTCCTTTCCA
BMM	AAGTATGCACCGCATCTGTTG	CAAATCGCAGAGGAGACAGC
sws/CG2212	CTGGATGGCGGCTATGTGAATAA	CCATTTCTTGTAGAGCAGCCAC
Cct1	TCCACCTCGCAGCAATTCTTC	GTAGTCACATCTATCCCGCTCC
Fatp	GAAATCCTTCTCGCGAATTCCT	GGAGATGAAAGCCATATCGCC
Rfabg	GGTTTCTGGCATATTGTTGA	TAGGGTGCGTATGCC ATCAA
DUOX	GCTGCACGCCAACCACAAGAGACT	CACGCGCAGCAGGATGTAAGGTTT
mrt	GGAGGATATTCTCGGAGTGGAGC	GCTTCCTGCCTCGTAGTCGAAC
pzg	GCTGAGGAACCACAACCATCTGAC	GTAACCTCGCCTTCGCCAGATT
Primers for plasmid construction and dsRNA synthesis		
F-*mrt*(RelB)-luc	CGAGATCTGCGATCTAAGTATAACG TCGTAGCGCACACGCACACC	CAGTACCGGAATGCCAAGCTGGGT GCACCCTTTGATCAAGGTCTT
pzg-luc	CGAGATCTGCGATCTAAGTACACAG TAGCAGCACAACGGAGACG	CAGTACCGGAATGCCAAGCTCTGT AGCAGTTCTCGACGGACGCGT
T-*mrt*(RelB)-luc	CGAGATCTGCGATCTAAGTAGCCAC TTTGTCGCAGTGTATCTGT	CAACAGTACCGGAATGCCAGCTGG GTGCACCCTTTGATCAAG
T-*mrt*-luc	CGAGATCTGCGATCTAAGTACGTTA GCTTTTTGCTGTCATTCGT	CCAACAGTACCGGAATGCCAGATG CTGTTGGAAAACAAGCAA
dsRelish	TAATACGACTCACTATAGGGAGATC AAACACGTGCCGC	TAATACGACTCACTATACCCAGACT CACGCTCTGTCTC
dsGFP	TAATACGACTCACTATAGGGAGAAT GGTGAGCAAGGGCGAGGA	TAATACGACTCACTATAGGGAGACT TGTACAGCTCGTCCATGC

334

335